Cell Reports

Article

MOF-mediated acetylation of SIRT6 disrupts SIRT6-FOXA2 interaction and represses SIRT6 tumor-suppressive function by upregulating ZEB2 in NSCLC

Graphical abstract

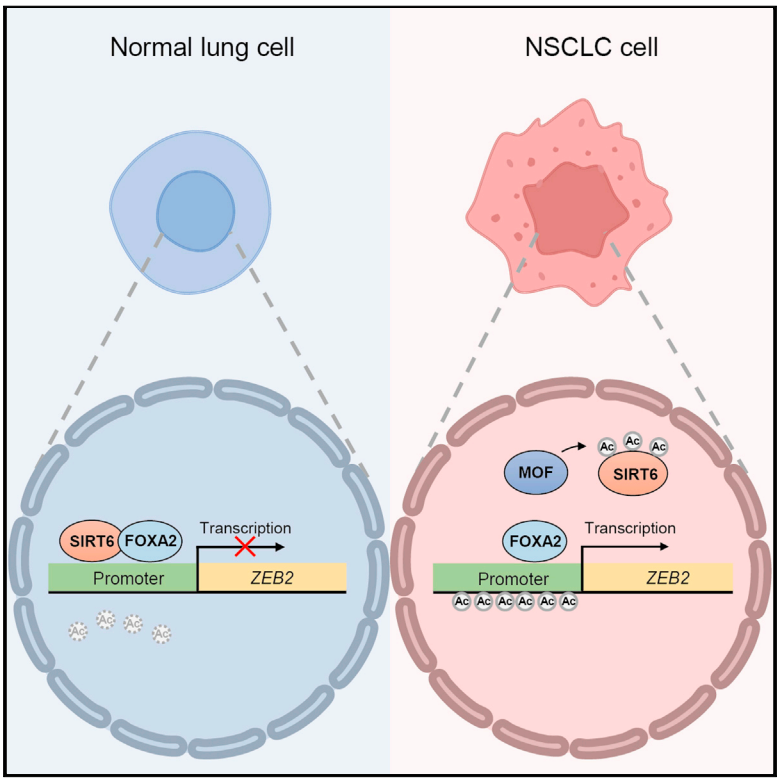

Highlights

- MOF acetylates SIRT6 at K128, K160, and K267, which is counteracted by HDAC1
- Acetylation by MOF impairs SIRT6 deacetylase activity
- MOF-mediated acetylation impairs the tumor-suppressive function of SIRT6 in NSCLC
- Acetylation of SIRT6 disrupts SIRT6-FOXA2 interaction and promotes ZEB2 expression in NSCLC

Authors

Kaiqiang Zhao, Mingyue Zheng, Zezhuo Su, ..., Joshua Wing Kei Ho, Guoxiang Jin, Zhongjun Zhou

Correspondence

gxjinking@163.com (G.J.), zhongjun@hku.hk (Z.Z.)

In brief

Zhao et al. show that the tumor-suppressive function of SIRT6 in NSCLC is regulated by MOF. MOF-mediated acetylation disrupts the SIRT6-FOXA2 interaction and promotes the transcriptional activation of *ZEB2*, which in turn potentiates NSCLC. These findings suggest the MOF-SIRT6-ZEB2 axis may serve as a promising therapeutic target in NSCLC.

Zhao et al., 2023, Cell Reports *42*, 112939
August 29, 2023
https://doi.org/10.1016/j.celrep.2023.112939

CellPress

Cell Reports

CellPress
OPEN ACCESS

Article

MOF-mediated acetylation of SIRT6 disrupts SIRT6-FOXA2 interaction and represses SIRT6 tumor-suppressive function by upregulating ZEB2 in NSCLC

Kaiqiang Zhao,[1,2,4] Mingyue Zheng,[1] Zezhuo Su,[2,6] Shrestha Ghosh,[2,7] Chao Zhang,[3] Wenzhao Zhong,[3] Joshua Wing Kei Ho,[2,6] Guoxiang Jin,[1,*] and Zhongjun Zhou[1,2,4,5,8,*]

[1]Medical Research Center, Guangdong Cardiovascular Institute, Guangdong Provincial People's Hospital, Guangdong Academy of Medical Sciences, Guangzhou 510080, P.R. China
[2]School of Biomedical Sciences, The University of Hong Kong, Hong Kong SAR, P.R. China
[3]Guangdong Lung Cancer Institute, Guangdong Provincial Key Laboratory of Translational Medicine in Lung Cancer, Guangdong Provincial People's Hospital & Guangdong Academy of Medical Sciences, Guangzhou 510080, P.R. China
[4]Centre for Regenerative Medicine and Health, Hong Kong Institute of Science & Innovation, Chinese Academy of Sciences, Hong Kong SAR, P.R. China
[5]Reproductive Medical Center, The University of Hong Kong Shenzhen Hospital, Shenzhen, P.R. China
[6]Laboratory of Data Discovery for Health Limited (D24H), Hong Kong Science Park, Hong Kong SAR, P.R. China
[7]Dana-Farber Cancer Institute, Harvard Medical School, Boston, MA, USA
[8]Lead contact
*Correspondence: gxjinking@163.com (G.J.), zhongjun@hku.hk (Z.Z.)
https://doi.org/10.1016/j.celrep.2023.112939

SUMMARY

Mammalian sirtuin 6 (SIRT6) regulates a spectrum of vital biological processes and has long been implicated in the progression of cancer. However, the mechanisms underlying the regulation of SIRT6 in tumorigenesis remain elusive. Here, we report that the tumor-suppressive function of SIRT6 in non-small cell lung cancer (NSCLC) is regulated by acetylation. Specifically, males absent on the first (MOF) acetylates SIRT6 at K128, K160, and K267, resulting in a decreased deacetylase activity of SIRT6 and attenuated SIRT6 tumor-suppressive function in NSCLC. Mechanistically, MOF-mediated SIRT6 acetylation hinders the interaction between SIRT6 and transcriptional factor FOXA2, which in turn leads to the transcriptional activation of *ZEB2*, thus promoting NSCLC progression. Collectively, these data indicate an acetylation-dependent mechanism that modulates SIRT6 tumor-suppressive function in NSCLC. Our findings suggest that the MOF-SIRT6-ZEB2 axis may represent a promising therapeutic target for the management of NSCLC.

INTRODUCTION

The mammalian sirtuin protein family includes a set of highly conserved NAD^+-dependent enzymes (sirtuins 1–7) with different subcellular localization, substrates, and biological functions. Among the seven mammalian sirtuins, sirtuin 6 (SIRT6) is predominantly localized in the nucleus and has been shown to regulate a spectrum of biological processes ranging from DNA-damage repair to genome maintenance, epigenetic regulation, metabolic homeostasis, inflammatory response, stem cell homeostasis, tumorigenesis, and aging.[1–3] SIRT6 predominantly functions as a deacetylase targeting both histone and non-histone proteins. The specific histone substrates for SIRT6 deacetylation include acetylated histone H3 lysine 9 (H3K9ac), H3K56ac, and H3K18ac, through which SIRT6 can regulate the promoter accessibility of specific genes and silence their transcription.[4–8] Human SIRT6 contains three main structural domains: the N terminus, a conserved core catalytic domain, and the C terminus. The N terminus is crucial for SIRT6 chromatin association and histone deacetylase activity, whereas the core catalytic domain is essential for the enzymatic activity of SIRT6. The C terminus contains a nuclear localization signal (NSL) and is critical for its proper nuclear localization.[9] Despite the extensive studies focusing on the biological functions of SIRT6, it remains largely unknown how SIRT6 activity is regulated in specific biological processes.

SIRT6 has been implicated in cancer progression by acting as a tumor suppressor mainly through its deacetylase activity.[10] Mechanistically, SIRT6 deacetylates H3K9ac and H3K56ac to co-represses the transcriptional programs of certain transcription factors, such as HIF1α and MYC, therefore inhibiting tumorigenesis in multiple types of cancer.[6,7,11] Lung cancer is the second most frequently diagnosed cancer and the leading cause of cancer-related mortality, accounting for 18% of the total cancer deaths worldwide in 2020.[12] Non-small cell lung cancer (NSCLC) represents the major type of lung cancer, accounting for more

than 80% of all cases. SIRT6 has been shown to exhibit tumor-suppressive properties in NSCLC.[13,14] More recently, it was also reported that pharmacological activation of SIRT6 using an allosteric SIRT6 activator, MDL-800, is sufficient to repress cell proliferation of NSCLC cells and decrease *in vivo* xenograft tumor formation.[15] Despite the appreciable progress in our understanding of the critical role of SIRT6 in NSCLC progression, the regulation of SIRT6 in the context of NSCLC remains elusive.

Post-translational modification (PTM) is a mechanism for cells to enable a fast yet efficient modulation of protein function in response to complex cellular stimuli. Several PTMs have been identified on SIRT6, regulating a wide range of SIRT6 functions.[16–24] For instance, phosphorylation by JNK on serine 10 promotes the recruitment of SIRT6 to DNA breaks upon oxidative stress,[22] whereas phosphorylation on serine 338 promotes SIRT6 protein degradation.[21,24] On the other hand, ubiquitination is reported to regulate SIRT6 protein stability, and deubiquitination by USP10 and USP48 protects SIRT6 from proteasomal degradation.[17,18] In addition, SUMOylation of SIRT6 at the C terminus selectively impairs SIRT6 deacetylase activity toward H3K56ac and disrupts SIRT6 interaction with transcription factor MYC, which in turn promotes tumorigenesis.[19] The acetylation of SIRT6 on lysine 33 (K33) was reported recently to hinder its polymerization and recruitment to DNA breaks upon DNA damage.[20] However, the responsible acetyltransferase for SIRT6 acetylation is yet to be identified. In addition, how acetylation affects SIRT6 functions in other physiological and pathological conditions remains largely unexplored.

In this study, we showed that the deacetylase activity of SIRT6 is regulated by acetylation. Specifically, males absent on the first (MOF) can acetylate SIRT6 at three conserved lysine residues. Acetylation of SIRT6 impairs its deacetylase activity and tumor-suppressive function in NSCLC. By RNA sequencing (RNA-seq) analysis, we identified zinc-finger E-box binding homeobox 2 (*ZEB2*) as a downstream target of SIRT6 in NSCLC cells. Mechanistically, we revealed that SIRT6 serves as a co-repressor of transcription factor forkhead box protein A2 (FOXA2) to repress *ZEB2* transcription. Acetylation by MOF jeopardizes the interaction between SIRT6 and FOXA2, leading to transcriptional activation of *ZEB2* and therefore promoting NSCLC progression. Our study not only uncovers a novel mechanism by which the MOF-SIRT6-ZEB2 axis regulates the NSCLC progression but also suggests that MOF-mediated SIRT6 acetylation may serve as a potential prognostic indicator and therapeutic target for NSCLC.

RESULTS

SIRT6 is acetylated by MOF at K128, K160, and K267

To verify whether SIRT6 is an acetylated protein, we first determined the acetylation of exogenously expressed SIRT6 (Figure 1A) and endogenous SIRT6 (Figure 1B) in HEK293 cells treated with sodium butyrate (NaB), an inhibitor of histone deacetylase (HDAC) family deacetylases. Using antibodies specifically against pan-acetyl-lysine, we detected the prominent acetylation in both ectopic FLAG-tagged SIRT6 and endogenous SIRT6 (Figures 1A and 1B). In addition, the endogenous SIRT6 in HEK293 cells could be immunoprecipitated by antibodies against pan-acetyl-lysine (Figure 1C). Together, these results substantiated that SIRT6 is an acetylated protein. We next set out to identify the acetyltransferase of SIRT6. To this end, we co-expressed a variety of candidate acetyltransferases including MOF, p300, TIP60, and GCN5 together with FLAG-SIRT6 in HEK293 cells and examined their ability to induce SIRT6 acetylation. The results showed that SIRT6 acetylation was only observed in the presence of MOF and p300, with a more robust effect for MOF than p300 (Figure 1D). Importantly, increased SIRT6 acetylation was only observed when expressing wild-type (WT) MOF but not inactive mutant MOF (Mut, K274R) (Figure 1E). Similarly, acetylation of the endogenous SIRT6 was also significantly increased in the presence of Myc-MOF in HEK293 cells (Figure 1F), whereas knocking down MOF with a specific small interfering RNA (siRNA) markedly decreased the basal acetylation level of SIRT6 (Figure 1G). Similar results were observed in A549 human non-small cell lung carcinoma cell line (Figures S1A and S1B). Taken together, these results suggest that MOF is an acetyltransferase of SIRT6.

Next, we set out to determine the MOF-targeted acetylation sites on SIRT6. To this end, FLAG-SIRT6 was co-expressed with Myc-MOF in HEK293 cells, enriched by immunoprecipitation using anti-FLAG M2 beads, and subjected to tandem mass spectrometry (MS/MS) analysis. MS/MS analysis suggested several potential acetylated lysine residues on SIRT6 including lysine 17 (K17), K128, K160, K170, K245, K267, and K300 (for details, see Table S1). To pinpoint which lysine residue on SIRT6 is the major MOF-targeted site, we constructed a set of lysine (K) to arginine (R) mutants mimicking SIRT6 acetylation-deficient conditions by site-directed mutagenesis. WT or acetylation-deficient mutants FLAG-SIRT6 were then co-expressed with Myc-MOF in HEK293 cells, respectively, followed by immunoprecipitation with anti-FLAG M2 beads to determine the changes in acetylation. The results showed that cells with ectopic K128R, K160R, and K267R mutant FLAG-SIRT6 exhibited reduced acetylation compared to those with WT SIRT6, while expressing other FLAG-SIRT6 mutants did not result in significant changes in SIRT6 acetylation (Figure 1H). Next, we constructed double-lysine mutants of SIRT6 with various combinations of the three lysine sites and a triple-lysine mutant of SIRT6 with all three lysine residues changed to arginine (K3R) to determine their acetylation levels in the presence of Myc-MOF in HEK293 cells. As shown in Figure 1I, SIRT6 acetylation was significantly reduced in cells with either single- or double-lysine SIRT6 mutants compared to that with the WT SIRT6. The SIRT6 acetylation was barely detectable in cells expressing triple-lysine mutant (K3R) SIRT6. The attenuated SIRT6 acetylation was not due to the impaired interaction between SIRT6 and MOF, as both WT and K3R SIRT6 could efficiently pull down the ectopic Myc-MOF (Figure S1C). Interestingly, K128, K160, and K267 are residues all located in the core catalytic domain of SIRT6 and are highly conserved in SIRT6 across different species (Figures 1J and S1D), indicating that acetylation of SIRT6 at these residues may have potential important biological consequences. Taken together, these results demonstrated that MOF acetylates SIRT6 at highly conserved sites K128, K160, and K267.

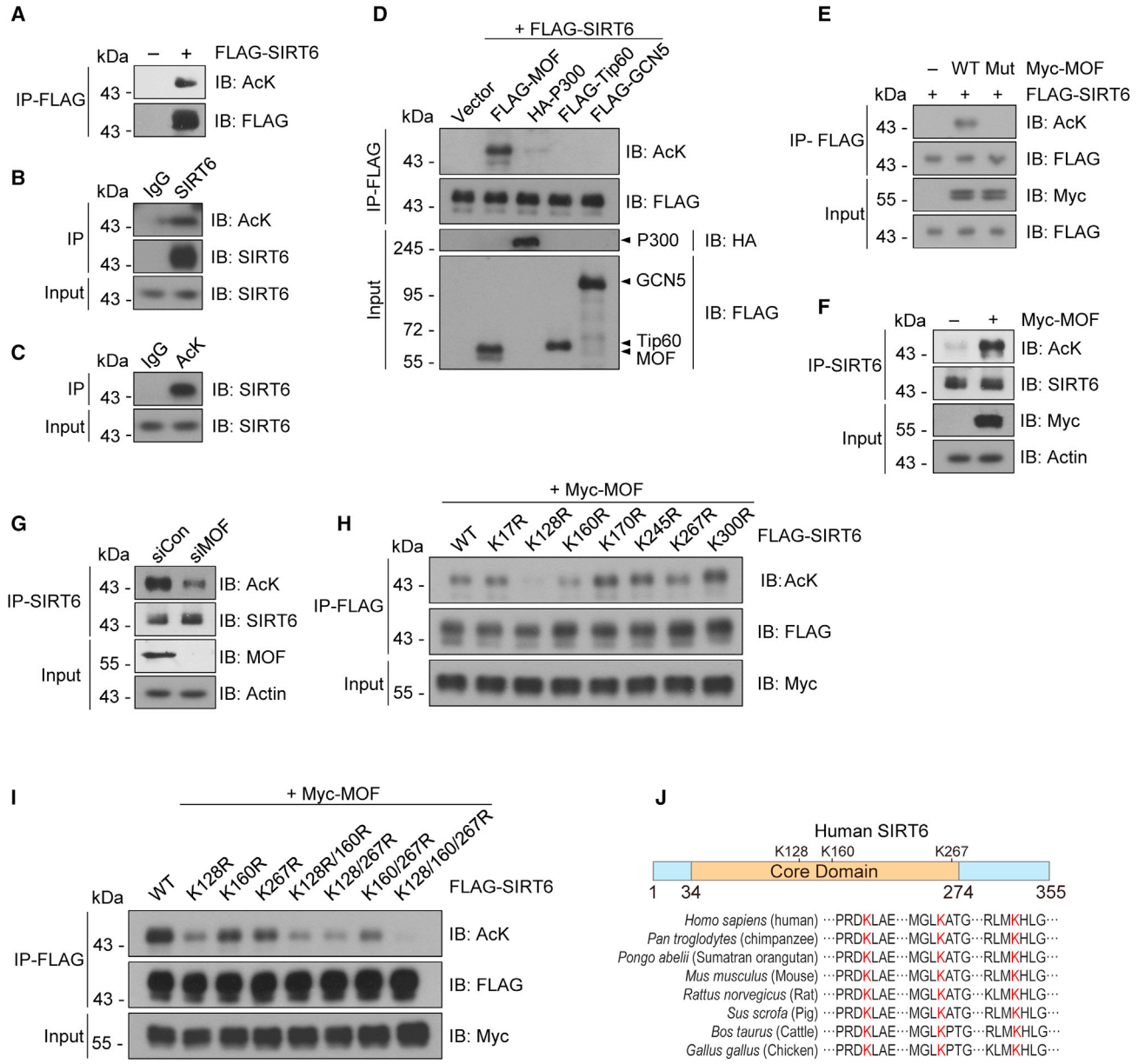

Figure 1. SIRT6 is acetylated by MOF at K128, K160, and K267

(A) HEK293 cells expressing FLAG-SIRT6 were treated with 1 mM sodium butyrate (NaB) for 24 h and subjected to immunoprecipitation (IP) with anti-FLAG beads. The precipitates were immunoblotted (IB) with anti-acetyl-lysine (AcK) and anti-FLAG antibodies.

(B and C) HEK293 cells were treated with 1 mM NaB for 24 h and subjected to immunoprecipitation with anti-SIRT6 antibodies or control immunoglobulin G (IgG) followed by immunoblotting with anti-acetyl-lysine and anti-SIRT6 antibodies (B) or with anti-acetyl-lysine antibody or control IgG followed by immunoblotting with anti-SIRT6 antibodies (C).

(D) FLAG-SIRT6 was co-expressed with different acetyltransferases in HEK293 cells for 48 h followed by immunoprecipitation with anti-FLAG beads. The precipitates were immunoblotted with anti-acetyl-lysine and anti-FLAG antibodies.

(E) FLAG-SIRT6 was co-expressed with Myc-MOF (wild-type [WT] or catalytically inactive mutant) in HEK293 cells. SIRT6 acetylation was examined by immunoprecipitation and immunoblotting as in (D).

(F) HEK293 cells transfected with Myc-MOF or Myc-tagged empty vector were lysed 48 h after transfection, and endogenous SIRT6 proteins were immunoprecipitated with anti-SIRT6 antibodies followed by immunoblotting with anti-acetyl-lysine and anti-SIRT6 antibodies.

(G) HEK293 cells transfected with control siRNA or siRNA specifically targeting MOF were immunoprecipitated by antibody against SIRT6. Acetylation of endogenous SIRT6 was examined by immunoblotting.

(H and I) Myc-MOF was co-expressed with either WT or indicted mutant FLAG-SIRT6 in HEK293 cells. The acetylation of FLAG-SIRT6 was examined as in (D).

(J) (Top) Illustration of lysine residues targeted by MOF for acetylation in human SIRT6. (Bottom) Alignment of SIRT6 amino acid sequences from various species. Red letters highlight the conserved lysines across the different species.

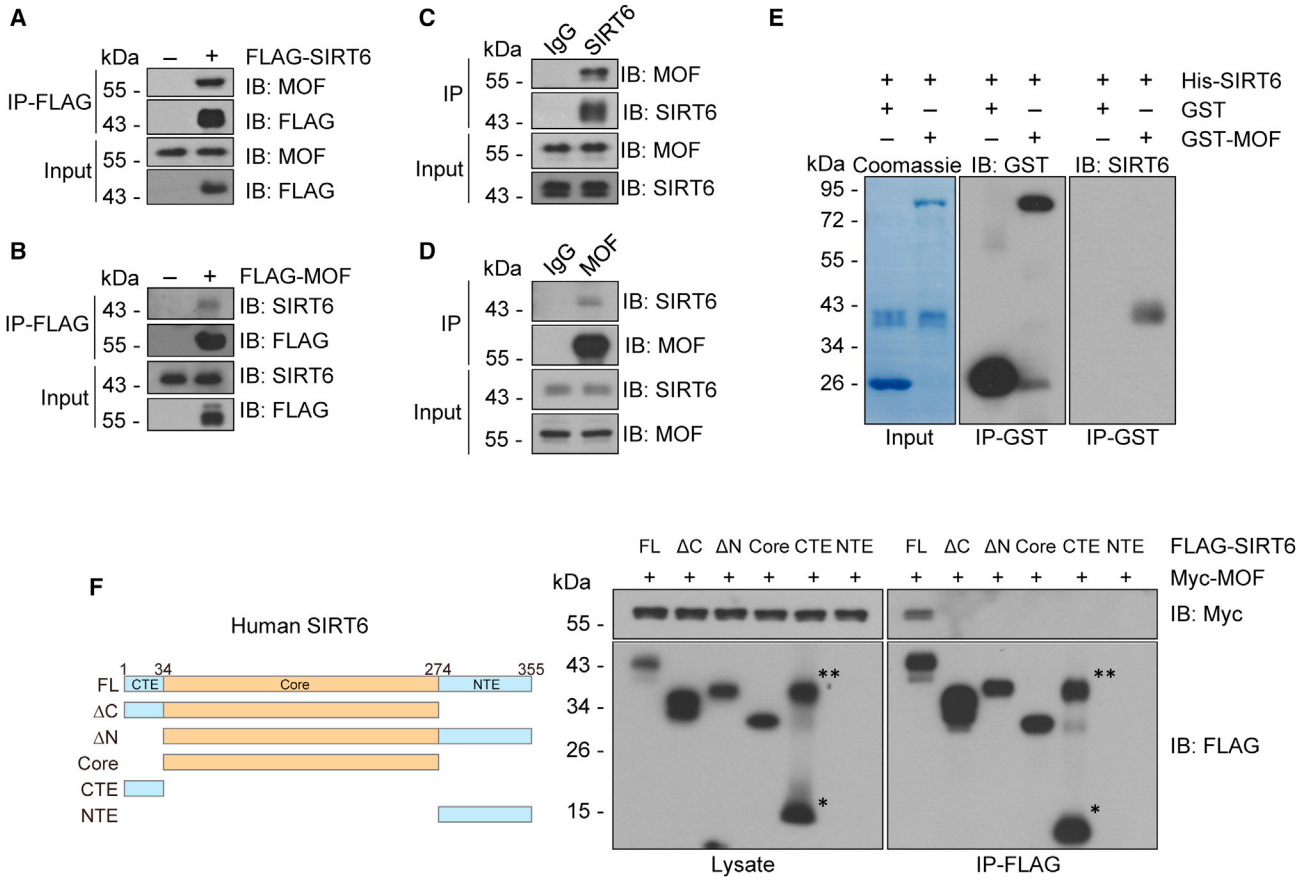

Figure 2. SIRT6 interacts with MOF

(A) FLAG-SIRT6 or FLAG-tagged empty vector was expressed in HEK293 cells. Whole-cell lysates were co-immunoprecipitated (IP) with anti-FLAG beads followed by immunoblotting (IB) with anti-MOF and anti-FLAG antibodies.

(B) Co-immunoprecipitation assays were carried out to determine the interaction between endogenous SIRT6 and ectopic MOF using a strategy similar to that in (A).

(C and D) Endogenous SIRT6 or MOF was immunoprecipitated with anti-SIRT6 (C) or anti-MOF antibodies (D) in HEK293 cells, followed by immunoblotting with antibodies against MOF and SIRT6.

(E) GST or GST-MOF was incubated with purified His-tagged SIRT6 and pulled down with glutathione-agarose beads. The immunoprecipitants were applied for western blotting assay using antibodies against GST or SIRT6. The purified recombinant proteins were visualized by Coomassie blue staining.

(F) (Left) Schematic diagram of SIRT6 domains and truncated mutants used in this study. WT or truncated mutant FLAG-SIRT6 was co-expressed with Myc-MOF in HEK293 cells, respectively. (Right) Co-immunoprecipitation was performed with anti-FLAG beads 48 h after transfection followed by immunoblotting with anti-Myc and anti-FLAG antibodies. FL, full-length SIRT6; ΔC, ΔN, C- or N-terminal domain deletion of SIRT6; Core, core domain of SIRT6; CTE, NTE, C- or N-terminal extension domain of SIRT6; single asterisks indicate CTE truncated SIRT6 protein; double asterisks indicate non-specific band.

SIRT6 interacts with MOF

Given that SIRT6 is acetylated by MOF, we next examined the potential interaction between the two proteins. We first ectopically expressed FLAG-SIRT6 in HEK293 cells and pulled down SIRT6 with anti-FLAG M2 beads. As shown in Figure 2A, endogenous MOF was pulled down together with FLAG-SIRT6. Reciprocally, endogenous SIRT6 was co-precipitated with FLAG-MOF by anti-FLAG M2 beads in HEK293 cells (Figure 2B). Next, to determine whether SIRT6 interacts with MOF under physiological conditions, we performed co-immunoprecipitation using specific antibodies against SIRT6 and MOF, respectively, to examine their endogenous interaction in HEK293 cells. As shown in Figures 2C and 2D, the endogenous MOF was co-precipitated with endogenous SIRT6 in HEK293 cells and vice versa. The endogenous interaction between SIRT6 and MOF was further confirmed in human NSCLC cell line A549 cells (Figure S1E). To further determine whether SIRT6 is in direct association with MOF, we performed an *in vitro* binding assay. Indeed, glutathione *S*-transferase (GST)-MOF but not GST was able to pull down SIRT6 *in vitro* (Figure 2E). These results suggest that SIRT6 directly interacts with MOF.

To map the region of SIRT6 involved in the interaction with MOF, we ectopically expressed different domain-deleted SIRT6 mutants (Figure 2F, left panel) in HEK293 cells and examined their interaction with Myc-MOF. The N-terminal extension domain (NTE) of SIRT6 was hardly detectable. Consistent with our previous results, full-length SIRT6 could efficiently pull down Myc-MOF. However, removing either the C- or N-terminal

domains of SIRT6 (ΔC or ΔN, respectively) was sufficient to abrogate the interaction between SIRT6 and MOF. Notably, the core domain (Core) or C-terminal extension domain (CTE) of SIRT6 alone failed to pull down Myc-MOF (Figure 2F, right panel). These results suggest that full-length SIRT6 is required for its interaction with MOF.

HDAC1 interacts with and deacetylates SIRT6

As acetylation is a reversible and dynamic process, we set out to identify the deacetylase of SIRT6. We first observed that the acetylation of ectopic FLAG-SIRT6 in HEK293 cells was markedly increased in the presence of NaB, an inhibitor of HDAC family deacetylases, rather than nicotinamide (NAM), an inhibitor of sirtuin family deacetylases (Figure S2A). This observation indicated that SIRT6 may potentially be deacetylated by HDAC family deacetylases. We then co-expressed FLAG-SIRT6 with MOF in the presence of different histone deacetylases (HDAC1–5) in HEK293 cells and found that only HDAC1 could decrease the SIRT6 acetylation level (Figure S2B). Furthermore, WT but not activity-deficient mutant HDAC1 (Mut, H141A) decreased the MOF-induced acetylation of SIRT6 in HEK293 cells (Figure S2C, lanes 1–4). A previous study has shown that SIRT1, but not other sirtuin family deacetylases, could deacetylate SIRT6.[20] However, ectopic SIRT1 failed to decrease MOF-induced acetylation of SIRT6 in HEK293 cells and, as expected, overexpression of an activity-deficient mutant SIRT1 (Mut, H363Y) did not affect MOF-induced acetylation of SIRT6 (Figure S2C, lanes 5 and 6). To further confirm that HDAC1 is a deacetylase of SIRT6, we performed an *in vitro* deacetylation assay using recombinant His-HDAC1 and His-HDAC2. Notably, HDAC1 but not HDAC2 efficiently deacetylated SIRT6 *in vitro* (Figure S2D). Accordingly, knockout of *HDAC1* via the CRISPR-Cas9 system markedly increased the acetylation of FLAG-SIRT6 in HKE293 cells (Figure S2E). These results suggest that HDAC1 is a deacetylase of SIRT6.

Next, we assessed the potential interaction between SIRT6 and HDAC1. We first confirmed that endogenous HDAC1 was co-precipitated with FLAG-SIRT6 in HEK293 cells (Figure S2F). Importantly, the endogenous interaction between SIRT6 and HDAC1 was also observed in HEK293 cells and human NSCLC cell line A549 cells (Figures S1E, S2G, and S2H). Taken together, these results demonstrated that HDAC1 interacts with SIRT6 and deacetylates MOF-mediated SIRT6 acetylation.

Acetylation by MOF impairs SIRT6 deacetylase activity without affecting its nuclear localization and protein stability

We next sought to examine whether MOF-mediated acetylation affects SIRT6 protein property and function. To this end, we constructed a triple acetylation-mimetic mutant SIRT6 (K3Q) with all three MOF-targeted lysines (K) mutated to glutamines (Q) to mimic hyperacetylated SIRT6 at these sites. As shown in Figure S3A, immunofluorescence staining indicated that K3R and K3Q SIRT6 exhibited nuclear localization similar to that of WT SIRT6 in HEK293 cells. Thus, the acetylation status on MOF-targeted sites did not affect SIRT6 nuclear localization. As acetylation is reported to regulate protein stability,[25–27] we next examined whether acetylation by MOF also modulates the protein stability of SIRT6. HEK293 cells expressing FLAG-SIRT6 WT, K3R, or K3Q were treated with cycloheximide (CHX) to inhibit protein synthesis. Cell lysates were then collected at different time points upon CHX treatment and subjected to western blotting to check the protein abundance of FLAG-SIRT6. No significant difference in the degradation rates was found between SIRT6 WT and mutants (Figures 3A and 3B). Consistently, no obvious change was observed in the degradation rate of FLAG-SIRT6 in the presence or absence of Myc-MOF in HEK293 cells (Figures S3B and S3C), thus indicating that acetylation by MOF did not affect SIRT6 protein stability.

The localization of three MOF-targeted sites in the core catalytic domain of SIRT6 prompted us to speculate that the acetylation at these sites may affect SIRT6 deacetylase activity. To test this, we transfected HEK293 cells with FLAG-SIRT6 WT, HY (deacetylase-deficient H133Y mutant, as a negative control), K3R, or K3Q to examine their activities toward endogenous H3K9ac and H3K56ac histone marks, two well-established specific histone substrates of SIRT6 in cells.[4,28] As expected, WT but not the HY mutant SIRT6 markedly decreased the levels of H3K9ac and H3K56ac in cells (Figure 3C, lanes 1–4). Intriguingly, K3R SIRT6 efficiently decreased the H3K9ac and H3K56ac, whereas K3Q SIRT6 exhibited an attenuated deacetylase activity toward the two histone marks in HEK293 cells (Figure 3C). By employing purified FLAG-SIRT6 WT, HY, K3R, K3Q, and extracted histones, we also performed an *in vitro* deacetylase assay. Consistent with the observation in cells, WT and K3R SIRT6, but not HY and K3Q SIRT6, efficiently deacetylated H3K9ac and H3K56ac *in vitro* (Figure 3D). To explore which MOF-targeted site contributes to the impaired SIRT6 deacetylase activity, we purified the FLAG-tagged K128Q, K160Q, and K267Q SIRT6 proteins for the *in vitro* deacetylase assay. As shown in Figure S3D, the K128Q SIRT6 mutant exhibited a moderate inhibitory effect, whereas the K3Q mutant exhibited the highest inhibitory effect on SIRT6 deacetylase activity. Interestingly, the decreased H3K9ac and H3K56ac in HEK293 with ectopic SIRT6 was largely restored in cells with ectopic MOF expression, and this restoration was attenuated when HDAC1 was expressed (Figures 3E and S3E). Taken together, these data suggested that MOF-mediated acetylation impairs the deacetylase activity of SIRT6 without affecting its nuclear localization and protein stability.

Acetylation by MOF attenuates SIRT6 tumor-suppressive activity in NSCLC cells

It has been shown that the expression of SIRT6 is decreased in NSCLC patient tissues and cell lines, and activation of SIRT6 deacetylase activity was sufficient to attenuate the tumorigenic potential of NSCLC cells.[13–15] Interestingly, MOF has been shown to exhibit enhanced expression in NSCLC patient tissues,[29–33] indicating an oncogenic function of MOF in NSCLC. However, whether there is a link between increased expression of MOF and the activity of SIRT6 in NSCLC has not been examined.

Based on the above observations, we speculate that MOF-mediated acetylation may contribute to the attenuated tumor-suppressive activity of SIRT6 in NSCLC. To test this hypothesis, we first established two NSCLC cell lines (A549 and H1299)

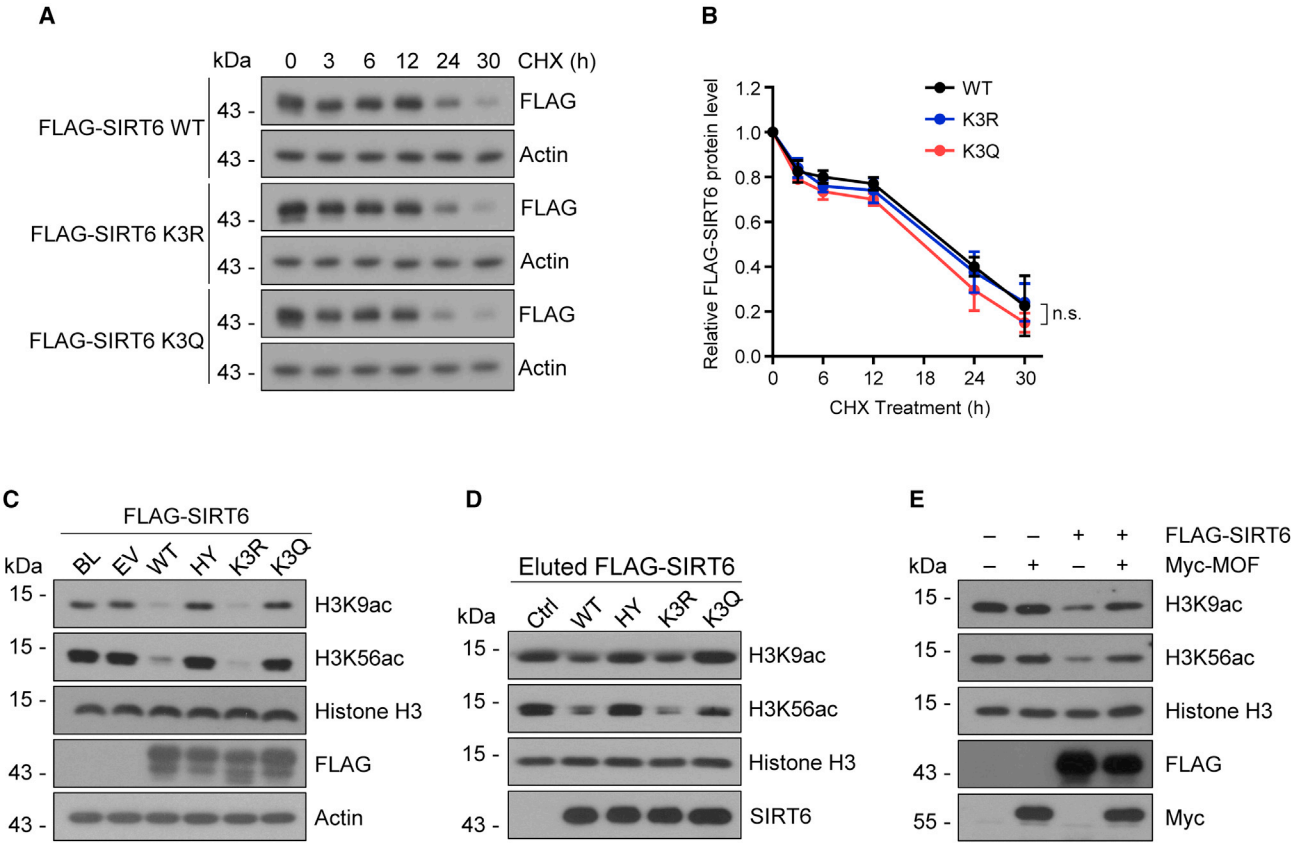

Figure 3. Acetylation by MOF impairs SIRT6 deacetylase activity without affecting its protein stability

(A) HEK293 cells expressing WT, K3R, or K3Q mutant FLAG-SIRT6 were treated with 300 μg/mL cycloheximide (CHX) for the indicated times. Cell lysates were then subjected to western blotting using antibodies against FLAG and actin.

(B) Quantification of the data as presented in (A) was carried out by ImageJ software. Data represent the mean ± SEM (n = 3), calculated using two-tailed Student's t test. n.s., not significant.

(C) HEK293 cells were transfected with FLAG-tagged empty vector (EV), FLAG-SIRT6 WT, HY, K3R, or K3Q mutant FLAG-SIRT6. Cell lysates were subjected to western blotting analysis using the indicated antibodies.

(D) Eluted WT, HY, K3R, or K3Q mutant FLAG-SIRT6 were incubated with extracted histone in the presence of NAD^+ followed by western blotting using antibodies as indicated.

(E) HEK293 cells expressing FLAG-SIRT6 or/and Myc-MOF were subjected to western blotting using antibodies as indicated.

stably expressing either control vector, FLAG-tagged WT, K3R, or K3Q SIRT6. Western blotting analysis confirmed that the expression of the different forms of FLAG-SIRT6 in the two NSCLC cell lines was comparable (Figure 4A). The functional consequences of different forms of FLAG-SIRT6 were tested in the two NSCLC cell lines. While the expression of WT and K3R SIRT6 significantly repressed the proliferation of the two NSCLC cell lines, this was not observed in cells with acetylation-mimetic K3Q SIRT6 (Figure 4B). Similarly, WT and K3R SIRT6, but not K3Q SIRT6, reduced the colony-formation potential of the two NSCLC cell lines (Figure 4C). In addition, cell-cycle analysis of H1299 cells showed that expression of WT and K3R SIRT6 led to a significant reduction in the percentage of cells in the S and G_2/M phases with a concomitant increase in the percentage of cells in the G_0/G_1 phase. However, K3Q SIRT6 exhibited no effect on the cell-cycle progression in H1299 cells (Figure 4D). Consistently, WT and K3R SIRT6, but not K3Q SIRT6, suppressed the migration and invasion of NSCLC cells (Figures 4E and 4F). These results suggested that hyperacetylation attenuates the tumor-suppressive function of SIRT6 in NSCLC cells.

To confirm whether the attenuated SIRT6 tumor-suppressive activity in NSCLC cells was indeed mediated by MOF, we stably expressed MOF in NSCLC cell lines with ectopic SIRT6. Western blotting analysis confirmed the successful expression of MOF in two NSCLC cell lines (Figure 5A). Consistent with the aforesaid results, MOF expression markedly increased the acetylation of FLAG-SIRT6 in two NSCLC cell lines (Figure 5A). SIRT6 significantly decreased the tumorigenic properties of NSCLC cells such as cell proliferation, colony-formation potential, and cell-cycle progression. While MOF alone did not affect any of these properties, the presence of both proteins markedly attenuated the suppressive ability of SIRT6 on these tumorigenic properties in NSCLC cells (Figures 5B–5D). In addition, the ability of SIRT6 to suppress migration and invasion in NSCLC cells was also significantly reduced in the presence of MOF (Figures 5E and

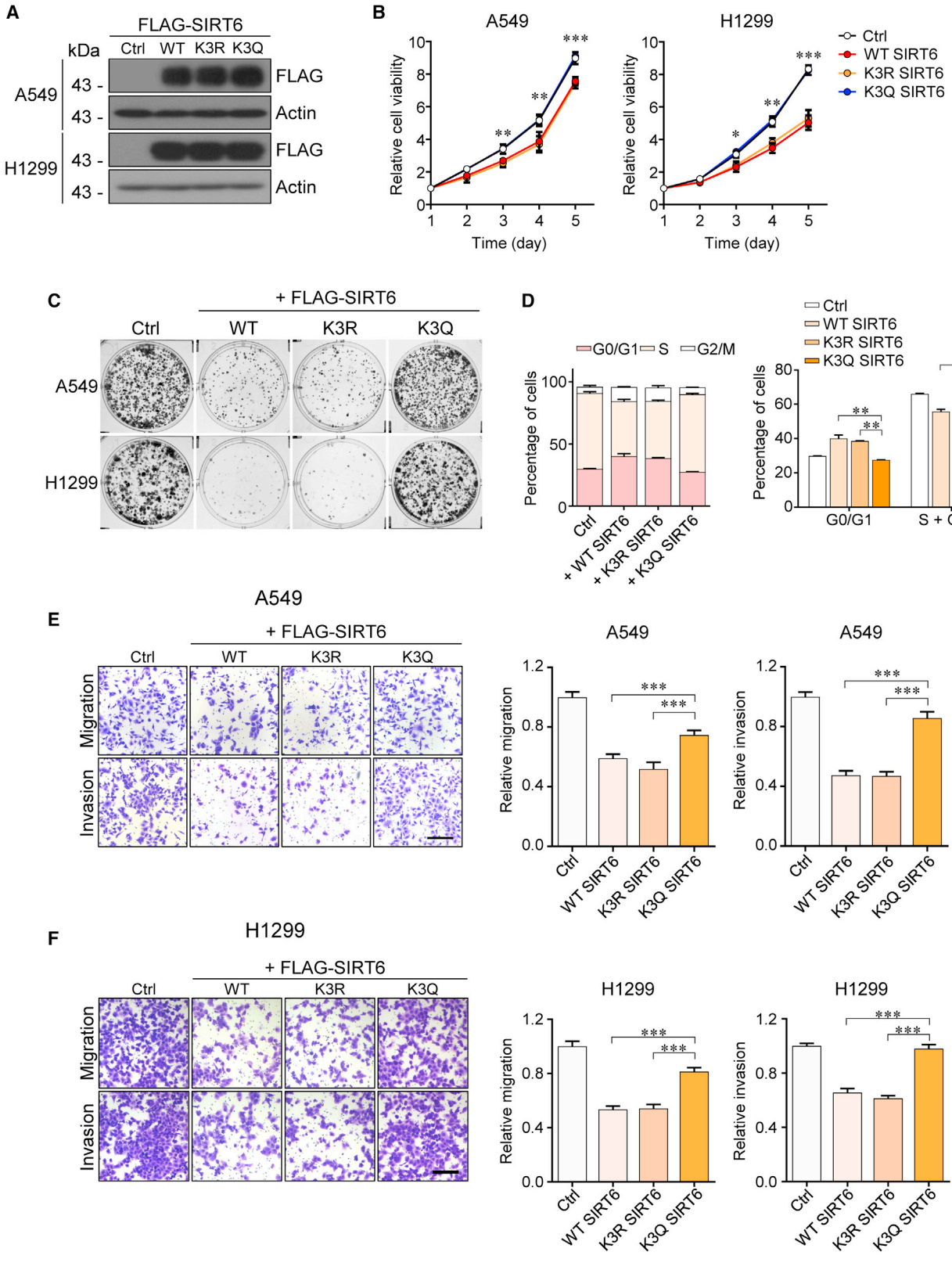

(legend on next page)

5F). Taken together, these results suggested that MOF-mediated acetylation attenuates the tumor-suppressive function of SIRT6 in NSCLC cells.

Acetylation by MOF attenuates SIRT6-mediated transcriptional repression of *ZEB2* in NSCLC cells

We next sought to elucidate the mechanism of how MOF-mediated acetylation attenuates the tumor-suppressive function of SIRT6 in NSCLC. Accumulating evidence suggests that SIRT6 exerts tumor-suppressive function through transcriptional suppression of downstream oncogenes. Intriguingly, SIRT6 seems to repress the transcription of specific downstream targets in different types of cancer.[7,11,34] Although SIRT6 exhibits tumor-suppressive activities in NSCLC,[13–15] the downstream targets of SIRT6 in NSCLC cells have not been systemically determined. To identify the SIRT6 target genes in NSCLC cells, total RNA from NSCLC cells expressing either control vector, FLAG-SIRT6 WT, K3R, or K3Q were extracted for RNA-seq analysis. The transcriptomic profiles were then compared between control and cells expressing different SIRT6 mutants. The differentially expressed genes are presented in Table S2. Interestingly, *ZEB2* was found among the top five differentially downregulated genes in WT or K3R SIRT6-expressing cells compared to control cells. However, the decreased expression of *ZEB2* was not observed in cells expressing K3Q SIRT6 compared to control cells (Figure 6A). This suggests that *ZEB2* is potentially targeted by SIRT6 in NSCLC cells and might be regulated by the acetylation status of SIRT6.

ZEB2 has been shown to implicate in NSCLC, and the suppression of *ZEB2* could inhibit the tumorigenic properties of NSCLC cells.[35–41] The reduced transcription of *ZEB2* in WT and K3R SIRT6-expressing NSCLC cells was further validated by qPCR, whereas such transcriptional repression of *ZEB2* was significantly attenuated in acetylation-mimetic K3Q SIRT6-expressing cells (Figure S4A). In line with this, acetylation-mimetic K3Q SIRT6 displayed a reduced ability in repressing ZEB2 protein expression in NSCLC cells (Figure S4B). In addition, we observed that the mRNA and protein levels of ZEB2 were significantly restored when MOF was introduced into NSCLC cells with stable SIRT6 expression, although expressing MOF alone has no impact on the expression of ZEB2 (Figures S4C and S4D). Moreover, analysis of mRNA expression using The Cancer Genome Atlas LUAD and LUSC (lung adenocarcinoma and lung squamous cell carcinoma) data cohorts revealed a significant negative correlation between *SIRT6* and *ZEB2* expression (Figure S4E). To test whether SIRT6 indeed suppresses tumorigenic properties of NSCLC cells through repressing *ZEB2*, we established A549 and H1299 NSCLC cells with stable knockdown of *ZEB2* (Figure S5A). Intriguingly, depleting *ZEB2* abolished the SIRT6 ability in repressing the colony-formation potential in NSCLC cell lines (Figure S5B). In addition, reconstitution of ZEB2 in SIRT6-expressing NSCLC cells partially restored the proliferation, colony formation, cell migration, and cell invasion of NSCLC cells suppressed by SIRT6 (Figure S6A–S6H). These results indicated that SIRT6 exerts its tumor-suppressive function, at least partially, through the transcriptional repression of *ZEB2* in NSCLC cells.

Taken together, these findings suggested that *ZEB2* is a downstream target of SIRT6 in NSCLC cells and that MOF-mediated acetylation attenuates SIRT6-repressive activity against *ZEB2* transcription.

Acetylation by MOF dampens the interaction between SIRT6 and FOXA2 and decreases SIRT6 recruitment to the promoter of *ZEB2*

We next sought to determine how SIRT6 suppresses the transcription of *ZEB2* in NSCLC cells and the role of MOF-mediated acetylation of SIRT6 in this process. It was previously reported that SIRT6 interacts with transcriptional factor FOXA2 and represses *ZEB2* transcription in hepatocellular carcinoma cells.[42] However, the underlying mechanism regarding how SIRT6 cooperates with FOXA2 to repress *ZEB2* transcription and how MOF regulates such a process remain elusive. To test whether acetylation by MOF affects the interaction between SIRT6 and FOXA2, we performed co-immunoprecipitation assays to examine the interaction between FLAG-tagged WT, K3R, or K3Q SIRT6 with endogenous FOXA2 in A549 cells. As shown in Figure 6B, K3Q SIRT6 exhibited a reduced binding capability with endogenous FOXA2 compared to that of WT and K3R SIRT6. The interaction between FLAG-SIRT6 and endogenous FOXA2 in A549 cells was largely impaired in the presence of MOF, accompanied by enhanced acetylation of FLAG-SIRT6 (Figure 6C). Interestingly, expression of HDAC1 counteracted the reduced interaction between SIRT6 and FOXA2 induced by MOF (Figure S7A). These results indicated that MOF-mediated acetylation of SIRT6 jeopardizes the interaction between SIRT6 and FOXA2 in NSCLC cells.

It is well established that SIRT6 acts as a co-repressor of several transcriptional factors such as NF-κB,[5] c-Myc,[7] HIF1α,[6] and c-Jun,[43] facilitating the repression of downstream target genes by deacetylating H3K9ac and H3K56ac at the promoter regions. As SIRT6 interacts with FOXA2, it is plausible that SIRT6 may act as a co-repressor of FOXA2 and thus suppress *ZEB2* transcription by a similar mechanism. To test this hypothesis, we first performed chromatin immunoprecipitation (ChIP) analysis with anti-FLAG M2 beads followed by qPCR to evaluate

Figure 4. Acetylation-mimetic mutation of SIRT6 attenuates its tumor-suppressive activity in NSCLC cells

(A) Cell lysates from A549 and H1299 NSCLC cells with stable expression of control vector, WT, or various mutant SIRT6 were subjected to western blotting using antibodies against FLAG and actin.

(B and C) A549 and H1299 cells with stable expression of indicated plasmids were examined for cell viability over 5 days (B) and *in vitro* colony formation (C). Data represent mean ± SEM (n = 3), calculated using two-tailed Student's t test. *p < 0.05, **p < 0.01, ***p < 0.001.

(D) H1299 cells with stable expression of indicated plasmids were subjected to cell-cycle analysis. Data represent mean ± SEM (n = 3), calculated using two-tailed Student's t test. **p < 0.01.

(E and F) A549 (E) and H1299 (F) cells with stable expression of indicated plasmids were examined for cell migration and cell invasion. (Left) Representative images. Scale bars, 200 μm. (Right) Data represent the mean ± SEM (n = 3), calculated using two-tailed Student's t test. *p < 0.05, **p < 0.01, ***p < 0.001.

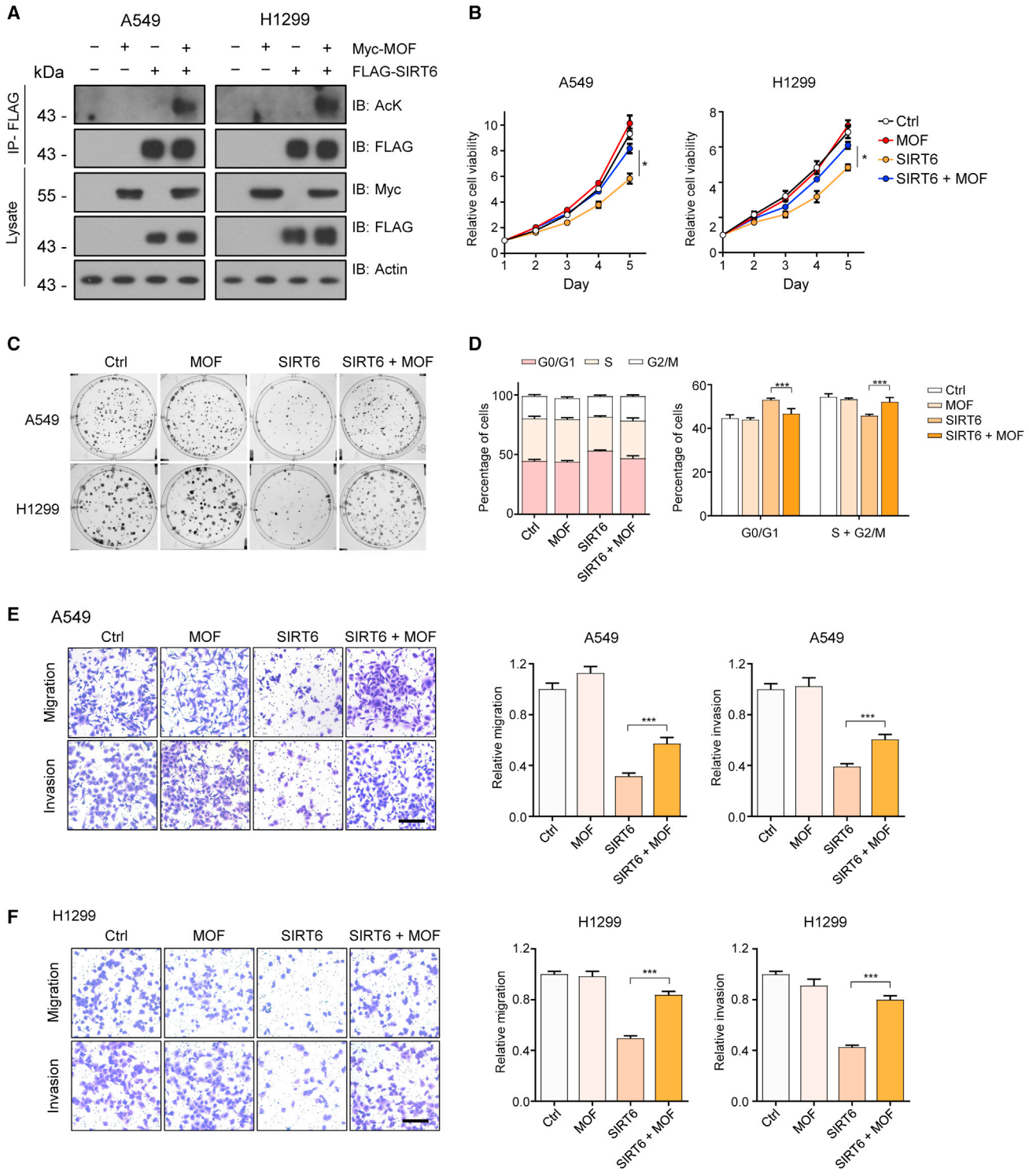

Figure 5. Acetylation by MOF attenuates SIRT6 tumor-suppressive function in NSCLC cells

(A) Cell lysates from A549 and H1299 cells with stable expression of indicated plasmids were subjected to immunoprecipitation with anti-FLAG beads; the precipitates and the whole-cell lysates were applied to western blotting analysis using indicated antibodies.

(B and C) A549 and H1299 cells generated in (A) were subjected to cell viability assay over 5 days (B) and *in vitro* colony-formation assay (C). Data represent mean ± SEM (n = 3), calculated using two-tailed Student's t test. *p < 0.05.

(legend continued on next page)

the binding of Flag-tagged WT and K3Q SIRT6 proteins to the promoter regions of *ZEB2* in A549 cells (Figure 6D). As shown in Figure 6E, while WT SIRT6 efficiently bound to the *ZEB2* promoter region, the acetylation-mimetic K3Q mutation significantly attenuated the association of SIRT6 with this locus, suggesting that acetylation of SIRT6 impairs its recruitment to the *ZEB2* promoter in NSCLC cells. As expected, the expression of WT or K3R SIRT6 markedly reduced H3K9ac and H3K56ac levels at the *ZEB2* promoter region (Figure 6F). In contrast, K3Q mutation significantly attenuated the reduction in H3K9ac and H3K56ac at the same locus (Figure 6F), most likely as a consequence of the reduced association of K3Q SIRT6 with the *ZEB2* promoter. In line with these observations, the association of SIRT6 with the *ZEB2* promoter was markedly attenuated in the presence of exogenous MOF (Figure 6G), accompanied by a significant increase of H3K9ac and H3K56ac levels at the same locus (Figure 6H). These data demonstrated that MOF-mediated acetylation impairs the binding of SIRT6 to the *ZEB2* promoter, leading to reduced deacetylation of H3K9ac and H3K56ac at *ZEB2* promoter regions.

Taken together, these results suggested that SIRT6 functions as a co-repressor of FOXA2 to suppress *ZEB2* transcription in NSCLC cells by deacetylating H3K9ac and H3K56ac at the *ZEB2* promoter region. MOF-mediated acetylation impairs the interaction between SIRT6 and FOXA2, leading to the decreased association of SIRT6 at the promoter of *ZEB2*, which in turn activates *ZEB2* transcription.

MOF-mediated acetylation impairs the tumor-suppressive efficacy of SIRT6 *in vivo*

We next sought to determine whether MOF-mediated acetylation decreases SIRT6 tumor-suppressive efficacy *in vivo* in NSCLC. To this end, H1299 cells stably expressing control vector, FLAG-tagged WT, K3R, or K3Q SIRT6 were inoculated subcutaneously into nude mice to allow tumor formation for 40 days. As shown in Figures 7A–7C, expression of WT or K3R SIRT6 substantially decreased the xenograft tumor formation in mice. However, acetylation-mimetic K3Q mutation attenuated such tumor-suppressive effects of SIRT6. Interestingly, depletion of MOF was able to enhance the ability of exogenous SIRT6 in repressing the colony-formation potential *in vitro* and the tumor-formation potential *in vivo* of the NSCLC cells (Figures S7B, S7C, and 7D–7F). These results indicated that MOF may affect the tumor-suppressive efficacy of SIRT6 both *in vitro* and *in vivo* in NSCLC through acetylation. Importantly, in agreement with the results *in vitro*, we also observed that depletion of *ZEB2* is sufficient to abolish the tumor-suppressive efficacy of exogenous SIRT6 *in vivo* (Figures 7G–7I). Together, these results demonstrated a role for the MOF-SIRT6-ZEB2 axis in regulating NSCLC progress.

In line with the data obtained from NSCLC cell lines, elevated SIRT6 acetylation with concomitant MOF expression was also observed in human NSCLC tumor samples (Figure 7J). In addition, preliminary results showed that increased acetylation of SIRT6 and MOF expression were observed in NSCLC tumor samples when compared with adjacent normal tissues (Figure 7K). These data provided further evidence for the critical role of SIRT6 in the development and progression of NSCLC through MOF-mediated acetylation, although further studies are necessary to systemically examine the potential correlation between the acetylation of SIRT6 and NSCLC progression.

DISCUSSION

In this study, we unveiled a novel mechanism by which SIRT6 tumor-suppressive function in NSCLC cells is regulated through MOF-mediated acetylation. Apart from MOF, p300 also induced SIRT6 acetylation to a lesser extent based on western blotting analysis (Figure 1D). However, whether p300 targets the same residues on SIRT6 remains unknown. Indeed, in addition to K128, K160, and K267, our mass spectrometry analysis suggested several other potential acetylated residues on SIRT6 such as K17, K170, K245, and K300. Therefore, it is plausible that p300 may target other residues on SIRT6 for acetylation. Interestingly, a previous report showed that SIRT6 is acetylated at K33.[20] However, K33 was not identified as an acetylated residue on SIRT6 by MOF in the present study. Therefore, this residue may not be the target of MOF or a major acetylation site of SIRT6 by MOF. Alternatively, p300 or other acetyltransferases not included in this study may potentially be responsible for SIRT6 K33 acetylation, which warrants further investigations. On the other hand, although SIRT1 was shown to deacetylate SIRT6 at K33,[20] our results show that SIRT1 failed to affect MOF-mediated acetylation of SIRT6. In contrast, we observed that HDAC1 could efficiently deacetylate MOF-mediated SIRT6 acetylation both in the cells and *in vitro*. These results indicated that different deacetylases may catalyze SIRT6 deacetylation at specific sites. Likewise, different acetyltransferases may target specific sites on SIRT6 for acetylation. These intriguing observations suggest that complex yet precise regulatory mechanisms may exist in cells to modulate SIRT6 activity and function in response to diverse cellular stimuli.

Higher nuclear expression of SIRT6 was reported to be associated with elevated overall survival rate in NSCLC patients.[44,45] However, contradictory results were also reported in a study comprising 12 NSCLC patients.[46] The fact that acetylation dampens SIRT6 tumor-suppressive function as observed in this study suggests that the level of SIRT6 expression alone may not necessarily reflect the functionality of SIRT6 in tumor growth and progression. The PTMs of SIRT6 should also be taken into consideration. On the other hand, even though many types of cancer have been observed to have reduced expression of MOF, increased expression of MOF has been shown in NSCLC[31–33] and likely promotes NSCLC development through direct regulation of *SKP2* transcription.[33] Based on the results from the current study, we propose a novel mechanism by which

(D) H1299 cells generated in (A) were subjected to cell-cycle analysis. Data represent mean ± SEM (n = 3), calculated using two-tailed Student's t test. ***p < 0.001.

(E and F) A549 (E) and H1299 (F) cells generated in (A) were examined for cell migration and cell invasion. (Left) Representative images. Scale bars, 200 μm. (Right) Data represent mean ± SEM (n = 3), calculated using two-tailed Student's t test, ***p < 0.001.

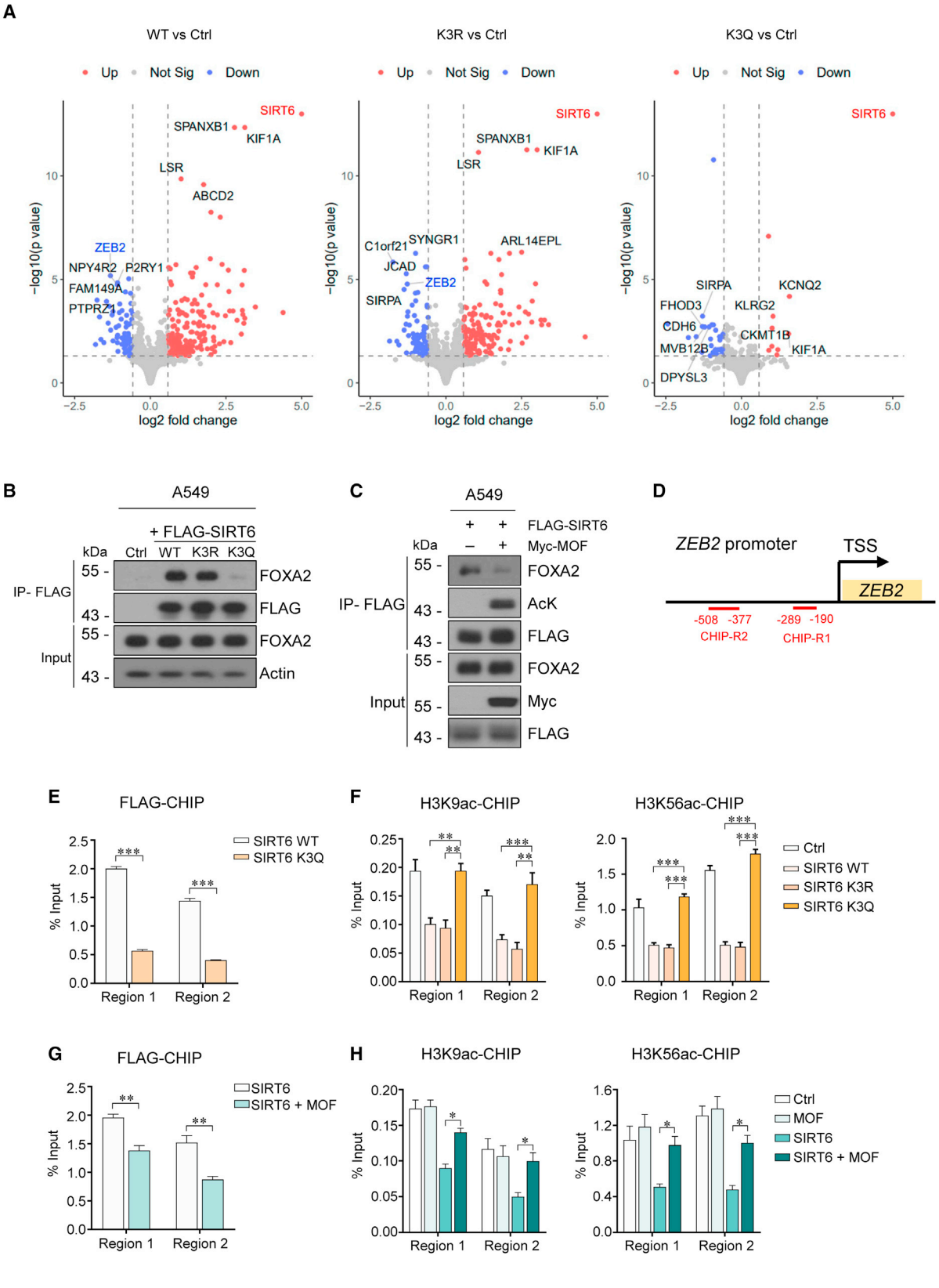

(legend on next page)

MOF acetylates and attenuates SIRT6 tumor-suppressive function in NSCLC. Specifically, MOF-mediated acetylation compromises the interaction between SIRT6 and FOXA2, resulting in increased H3K9ac and H3K56ac at the *ZEB2* promoter, which in turn transcriptionally activates *ZEB2*, thereby promoting the tumorigenic properties of NSCLC cells (Figure 7L). Thus, our findings uncovered an alternative mechanism by which MOF potentiates NSCLC progression through post-translational modulation of SIRT6.

Accumulating evidence indicates that SIRT6 may transcriptionally inhibit specific downstream genes in specific cancer types to achieve its tumor-suppressive function.[7,11,34] Surprisingly, the downstream targets of SIRT6 in NSCLC cells have not been systemically determined. In this study, we identified *ZEB2* as a potential downstream target of SIRT6 in NSCLC cells. Compared to WT SIRT6, acetylation-mimetic K3Q SIRT6 exhibited a reduced ability to repress *ZEB2* transcription in two NSCLC cells lines, suggesting that the repressive effect of SIRT6 on *ZEB2* is regulated by its acetylation status. It is worth noting that reconstitution of ZEB2 only partially eliminated the SIRT6 tumor-suppressive function in NSCLC cells, indicating that SIRT6 may suppress NSCLC progression by modulating genes other than *ZEB2*. Indeed, our RNA-seq analysis also identified several other genes that may potentially be repressed by SIRT6 in NSCLC such as *CSF1*, the downregulation of which has been shown to inhibit NSCLC cell proliferation and *in vivo* bone invasion.[47] Future studies are necessary to determine whether SIRT6 can modulate other genes including *CSF1* in NSCLC cells.

In this study, we showed that SIRT6 interacts with FOXA2 and acts as a co-repressor to repress *ZEB2* transcription in NSCLC cells. Acetylation by MOF dampened the interaction between SIRT6 and FOXA2, thereby activating *ZEB2* transcription. Acetylation is known to disrupt protein-protein binding as seen in the regulation of p53-SET interaction.[48] Therefore, acetylation may block the interacting surface of SIRT6 with FOXA2 by neutralizing the positive charge of K128, K160, and K267 on SIRT6, thus hindering the interaction between the two proteins. The ultimate elucidation of the mechanism underlying the disrupted interaction between SIRT6 and FOXA2 requires structural analysis of the complex. FOXA2 is a transcriptional factor that plays a regulatory role in multiple biological processes such as early development, metabolism homeostasis, and tumor metastasis.[49,50] As SIRT6 is also implicated in these processes and may act as a co-repressor of FOXA2, it will be of great interest to investigate whether SIRT6 also synergistically cooperates with FOXA2 to regulate the transcription of FOXA2-targeted genes in other biological processes.

In the current study, we observed increased SIRT6 acetylation with concomitant higher MOF expression in NSCLC patient tumor samples compared to the adjacent normal tissues (Figure 7K). These results, though preliminary, indicated that potential increased SIRT6 acetylation and higher expression of MOF may promote NSCLC development. Together with the data obtained from A549 and H1299 cell lines, these results may suggest a potential therapeutic implication. For instance, the levels in MOF expression and SIRT6 acetylation may serve as a prognostic indicator for NSCLC. On the other hand, interference in the interaction between MOF and SIRT6 by small molecules may provide an effective therapeutic strategy in the treatment of NSCLC, especially in patients with high MOF-expression levels. Thus, the MOF-SIRT6-FOXA2-ZEB2 axis may represent a promising target in drug screening for NSCLC.

Taken together, the results of this study demonstrated that MOF is an acetyltransferase for SIRT6. MOF-mediated SIRT6 acetylation significantly inhibited SIRT6 deacetylase activity without affecting its nuclear localization and protein stability. Functionally, acetylation by MOF attenuated SIRT6 tumor-suppressive activity in NSCLC by compromising the binding of SIRT6 with FOXA2, thus activating *ZEB2* transcription. Our findings provide insights into the development of new therapeutic strategies by targeting SIRT6 acetylation in NSCLC.

Limitations of the study

To identify the upstream acetyltransferase of SIRT6, we only tested the ability of MOF, p300, TIP60, and GCN5 on inducing SIRT6 acetylation in cells. However, there are more acetyltransferases apart from the tested ones and we cannot exclude the possibility that other untested acetyltransferases may also be able to acetylate SIRT6. Future studies may test whether other acetyltransferases also induce SIRT6 acetylation at other sites and investigate its biological functions. On the other hand, we only employed limited pairs of NSCLC patient tissues to check the MOF and SIRT6 acetylation levels. This is because the endogenous SIRT6 acetylation is extremely difficult to detect in

Figure 6. MOF-mediated acetylation dampens SIRT6 binding with FOXA2 and attenuates SIRT6 co-repressive activity against ZEB2 transcription

(A) Volcano plots showing global transcriptomic changes in WT vs. control (Ctrl), K3R vs. Ctrl, and K3Q vs. Ctrl determined by RNA-seq in A549 and H1299 cell lines. The top five differentially expressed genes (DEGs) were labeled. The full DEG dataset is listed in Table S2.

(B) Co-immunoprecipitation assay examining the interaction between FLAG-SIRT6 WT, K3R, or K3Q and the endogenous FOXA2 in A549 cells. FLAG-SIRT6 were pulled down with FLAG antibodies, and the immunoprecipitants were subjected to western blotting analysis using indicated antibodies.

(C) Co-immunoprecipitation assay examining the interaction between FLAG-SIRT6 and the endogenous FOXA2 in A549 cells in the presence or absence of Myc-MOF using a strategy similar to that in (B).

(D) Schematic representation of the ChIP-qPCR primer design within the human ZEB2 promoter region. TSS, transcription start site.

(E and F) ChIP-qPCR analysis of the occupancy of WT and K3Q mutant FLAG-SIRT6 (E) or H3K9ac and H3K56ac enrichment (F) at the promoter region of the ZEB2 gene in H1299 cells stably expressing the indicated plasmids. Data represent mean ± SEM (n = 3), calculated using two-tailed Student's t test. $^{**}p < 0.01$, $^{***}p < 0.001$.

(G) ChIP-qPCR analysis of the occupancy of FLAG-SIRT6 in the presence or absence of MOF expression in the promoter region of the ZEB2 gene in H1299 cells. Data represent mean ± SEM (n = 3), calculated using two-tailed Student's t test. $^{**}p < 0.01$.

(H) ChIP-qPCR analysis of H3K9ac and H3K56ac enrichment at the promoter region of the ZEB2 gene in the presence or absence of MOF expression in H1299 cells expressing FLAG-SIRT6. Data represent mean ± SEM (n = 3), calculated using two-tailed Student's t test. $^{*}p < 0.05$, $^{**}p < 0.01$.

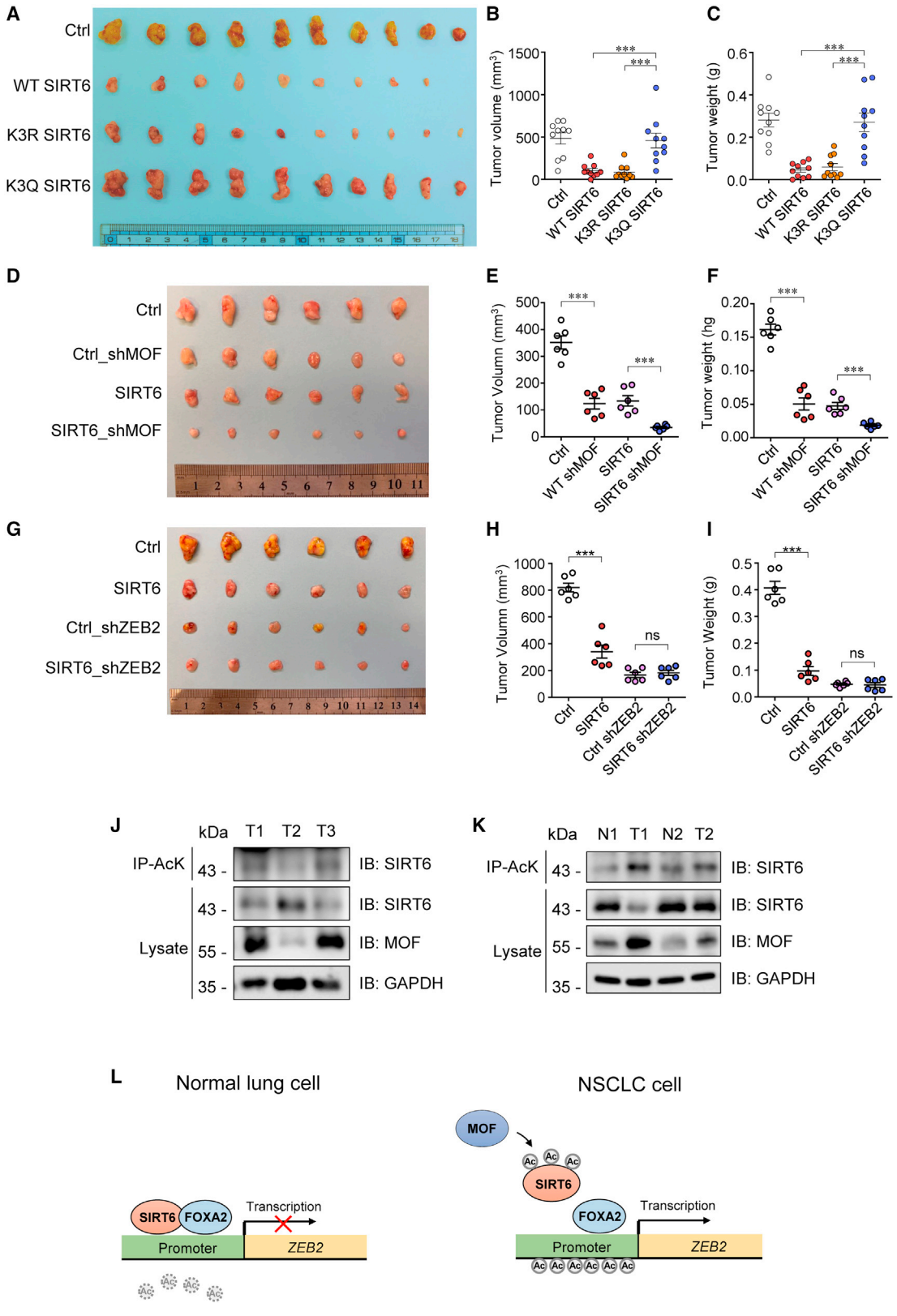

(legend on next page)

the patient tissues, and to maximally ensure that the results reflect the real *in vivo* situation, the tumor and the adjacent normal lung tissue samples were all freshly obtained from NSCLC patients who had just undergone surgery and were immediately applied to experiments. This largely limited the sample availability. Future studies should include more tissue samples to systemically test the potential correlation between the acetylation of SIRT6 and MOF expression and their relationship with NSCLC progression.

STAR★METHODS

Detailed methods are provided in the online version of this paper and include the following:

- KEY RESOURCES TABLE
- RESOURCE AVAILABILITY
  - Lead contact
  - Materials availability
  - Data and code availability
- EXPERIMENTAL MODEL AND SUBJECT DETAILS
  - NSCLC patient samples
  - Cell lines
- METHOD DETAILS
  - Plasmid constructs and siRNA
  - Co-immunoprecipitation and Western bolt
  - *In vitro* binding assay
  - Mass spectrometry-based identification of SIRT6 acetylation sites by MOF
  - Protein purification
  - *In vitro* deacetylation assay
  - Establishment of stable knockout cells using the CRISPR/Cas9 system
  - RNA-sequencing
  - Bioinformatics pipeline
  - Quantitative PCR
  - Immunofluorescence staining
  - Chromatin immunoprecipitation (ChIP) assay
  - Resazurin cell viability assay
  - *In vitro* colony formation assay
  - Propidium iodide staining and cell cycle analysis
  - *Trans*-well migration and invasion assays
  - *In vivo* xenograft tumorigenic assay
  - Patient tumor samples
- QUANTIFICATION AND STATISTICAL ANALYSIS
- ADDITIONAL RESOURCES

SUPPLEMENTAL INFORMATION

Supplemental information can be found online at https://doi.org/10.1016/j.celrep.2023.112939.

ACKNOWLEDGMENTS

We would like to thank Dr. Katrin Chua (Stanford University Medical Center) for kindly providing domain deletion mutants of SIRT6 plasmids and catalytically inactive SIRT6 plasmids and Dr. Lin Zhu for his help in MS/MS data visualization. We also thank Dr. Sheung Kin Ken Wong and Dr. Jin Wang for their help in the animal experiments, and Dr. Daniel Mak for proofreading the entire manuscript. This research was supported by the Innovation and Technology Commission of Hong Kong grant InnoHK@Health, Theme-based Research Scheme (T13-602/21N), Guangdong High-level Hospital Construction Project (KJ012019517), Guangdong Provincial People's Hospital Foundation (KY012021405), Science, Technology and Innovation Commission of Shenzhen Municipality (JCYJ20210324, 114408024 to Z.Z.), Guangdong Basic and Applied Basic Research Foundation (2021B1515130004) to Z.Z., and Innovation and Technology Commission of Hong Kong grant AIR@InnoHK to J.W.K.H.

AUTHOR CONTRIBUTIONS

Conceptualization, K.Z., S.G., and Z.Z.; methodology, K.Z., M.Z., Z.S., S.G., C.Z., J.W.K.H., and Z.Z.; investigation, K.Z., M.Z., and Z.S.; visualization, K.Z. and Z.S.; writing – original draft, K.Z. and Z.S.; writing – review & editing, J.W.K.H. and Z.Z.; funding acquisition, G.J., J.W.K.H., and Z.Z.; resources, W.Z., G.J., J.W.K.H., and Z.Z.; supervision, G.J., J.W.K.H., and Z.Z.

DECLARATION OF INTERESTS

The authors declare no competing interests.

Received: October 10, 2022
Revised: June 5, 2023
Accepted: July 20, 2023
Published: August 10, 2023

REFERENCES

1. Kugel, S., and Mostoslavsky, R. (2014). Chromatin and beyond: the multitasking roles for SIRT6. Trends Biochem. Sci. *39*, 72–81. https://doi.org/10.1016/j.tibs.2013.12.002.
2. Tasselli, L., Zheng, W., and Chua, K.F. (2017). SIRT6: Novel Mechanisms and Links to Aging and Disease. Trends Endocrinol. Metab. *28*, 168–185. https://doi.org/10.1016/j.tem.2016.10.002.
3. Korotkov, A., Seluanov, A., and Gorbunova, V. (2021). Sirtuin 6: linking longevity with genome and epigenome stability. Trends Cell Biol. *31*, 994–1006. https://doi.org/10.1016/j.tcb.2021.06.009.
4. Michishita, E., McCord, R.A., Boxer, L.D., Barber, M.F., Hong, T., Gozani, O., and Chua, K.F. (2009). Cell cycle-dependent deacetylation of telomeric histone H3 lysine K56 by human SIRT6. Cell Cycle *8*, 2664–2666. https://doi.org/10.4161/cc.8.16.9367.
5. Kawahara, T.L., Michishita, E., Adler, A.S., Damian, M., Berber, E., Lin, M., McCord, R.A., Ongaigui, K.C., Boxer, L.D., Chang, H.Y., and Chua, K.F. (2009). SIRT6 links histone H3 lysine 9 deacetylation to NF-kappaB-dependent gene expression and organismal life span. Cell *136*, 62–74. https://doi.org/10.1016/j.cell.2008.10.052.
6. Zhong, L., D'Urso, A., Toiber, D., Sebastian, C., Henry, R.E., Vadysirisack, D.D., Guimaraes, A., Marinelli, B., Wikstrom, J.D., Nir, T., et al. (2010). The

Figure 7. MOF-mediated acetylation impairs the tumor-suppressive efficacy of SIRT6 *in vivo*

(A–I) H1299 cells stably expressing indicated plasmids were subcutaneously injected into nude mice (A, D, and G). Tumors were dissected out 40 days later to determine the tumor volume (B, E, and H) and tumor weight (C, F, and I). Data represent mean ± SEM, calculated using two-tailed Student's t test. ***$p < 0.001$; ns, not significant.

(J and K) Whole tumor tissue lysates (J) or tumor tissues and their adjacent non-tumor tissue lysates (K) from NSCLC patients were applied to immunoprecipitation assays using anti-pan-acetyl-lysine antibodies, followed by western blotting assays using indicated antibodies.

(L) Working model of SIRT6 regulation by MOF through acetylation in normal and NSCLC cells.

histone deacetylase Sirt6 regulates glucose homeostasis via Hif1alpha. Cell *140*, 280–293. https://doi.org/10.1016/j.cell.2009.12.041.

7. Sebastián, C., Zwaans, B.M., Silberman, D.M., Gymrek, M., Goren, A., Zhong, L., Ram, O., Truelove, J., Guimaraes, A.R., Toiber, D., et al. (2012). The histone deacetylase SIRT6 is a tumor suppressor that controls cancer metabolism. Cell *151*, 1185–1199. https://doi.org/10.1016/j.cell.2012.10.047.
8. Tasselli, L., Xi, Y., Zheng, W., Tennen, R.I., Odrowaz, Z., Simeoni, F., Li, W., and Chua, K.F. (2016). SIRT6 deacetylates H3K18ac at pericentric chromatin to prevent mitotic errors and cellular senescence. Nat. Struct. Mol. Biol. *23*, 434–440. https://doi.org/10.1038/nsmb.3202.
9. Tennen, R.I., Berber, E., and Chua, K.F. (2010). Functional dissection of SIRT6: identification of domains that regulate histone deacetylase activity and chromatin localization. Mech. Ageing Dev. *131*, 185–192. https://doi.org/10.1016/j.mad.2010.01.006.
10. Kugel, S., Feldman, J.L., Klein, M.A., Silberman, D.M., Sebastián, C., Mermel, C., Dobersch, S., Clark, A.R., Getz, G., Denu, J.M., and Mostoslavsky, R. (2015). Identification of and Molecular Basis for SIRT6 Loss-of-Function Point Mutations in Cancer. Cell Rep. *13*, 479–488. https://doi.org/10.1016/j.celrep.2015.09.022.
11. Kugel, S., Sebastián, C., Fitamant, J., Ross, K.N., Saha, S.K., Jain, E., Gladden, A., Arora, K.S., Kato, Y., Rivera, M.N., et al. (2016). SIRT6 Suppresses Pancreatic Cancer through Control of Lin28b. Cell *165*, 1401–1415. https://doi.org/10.1016/j.cell.2016.04.033.
12. Sung, H., Ferlay, J., Siegel, R.L., Laversanne, M., Soerjomataram, I., Jemal, A., and Bray, F. (2021). Global Cancer Statistics 2020: GLOBOCAN Estimates of Incidence and Mortality Worldwide for 36 Cancers in 185 Countries. CA Cancer J. Clin. *71*, 209–249. https://doi.org/10.3322/caac.21660.
13. Han, Z., Liu, L., Liu, Y., and Li, S. (2014). Sirtuin SIRT6 suppresses cell proliferation through inhibition of Twist1 expression in non-small cell lung cancer. Int. J. Clin. Exp. Pathol. *7*, 4774–4781.
14. Wang, J., Sheng, Z., and Cai, Y. (2018). SIRT6 overexpression inhibits HIF1α expression and its impact on tumor angiogenesis in lung cancer. Int. J. Clin. Exp. Pathol. *11*, 2940–2947.
15. Shang, J.L., Ning, S.B., Chen, Y.Y., Chen, T.X., and Zhang, J. (2021). MDL-800, an allosteric activator of SIRT6, suppresses proliferation and enhances EGFR-TKIs therapy in non-small cell lung cancer. Acta Pharmacol. Sin. *42*, 120–131. https://doi.org/10.1038/s41401-020-0442-2.
16. Ronnebaum, S.M., Wu, Y., McDonough, H., and Patterson, C. (2013). The ubiquitin ligase CHIP prevents SirT6 degradation through noncanonical ubiquitination. Mol. Cell Biol. *33*, 4461–4472. https://doi.org/10.1128/mcb.00480-13.
17. Lin, Z., Yang, H., Tan, C., Li, J., Liu, Z., Quan, Q., Kong, S., Ye, J., Gao, B., and Fang, D. (2013). USP10 antagonizes c-Myc transcriptional activation through SIRT6 stabilization to suppress tumor formation. Cell Rep. *5*, 1639–1649. https://doi.org/10.1016/j.celrep.2013.11.029.
18. Du, L., Li, Y., Kang, M., Feng, M., Ren, Y., Dai, H., Wang, Y., Wang, Y., and Tang, B. (2021). USP48 Is Upregulated by Mettl14 to Attenuate Hepatocellular Carcinoma via Regulating SIRT6 Stabilization. Cancer Res. *81*, 3822–3834. https://doi.org/10.1158/0008-5472.Can-20-4163.
19. Cai, J., Zuo, Y., Wang, T., Cao, Y., Cai, R., Chen, F.L., Cheng, J., and Mu, J. (2016). A crucial role of SUMOylation in modulating Sirt6 deacetylation of H3 at lysine 56 and its tumor suppressive activity. Oncogene *35*, 4949–4956. https://doi.org/10.1038/onc.2016.24.
20. Meng, F., Qian, M., Peng, B., Peng, L., Wang, X., Zheng, K., Liu, Z., Tang, X., Zhang, S., Sun, S., et al. (2020). Synergy between SIRT1 and SIRT6 helps recognize DNA breaks and potentiates the DNA damage response and repair in humans and mice. Elife *9*. https://doi.org/10.7554/eLife.55828.
21. Thirumurthi, U., Shen, J., Xia, W., LaBaff, A.M., Wei, Y., Li, C.W., Chang, W.C., Chen, C.H., Lin, H.K., Yu, D., and Hung, M.C. (2014). MDM2-mediated degradation of SIRT6 phosphorylated by AKT1 promotes tumorigenesis and trastuzumab resistance in breast cancer. Sci. Signal. *7*, ra71. https://doi.org/10.1126/scisignal.2005076.
22. Van Meter, M., Simon, M., Tombline, G., May, A., Morello, T.D., Hubbard, B.P., Bredbenner, K., Park, R., Sinclair, D.A., Bohr, V.A., et al. (2016). JNK Phosphorylates SIRT6 to Stimulate DNA Double-Strand Break Repair in Response to Oxidative Stress by Recruiting PARP1 to DNA Breaks. Cell Rep. *16*, 2641–2650. https://doi.org/10.1016/j.celrep.2016.08.006.
23. Gao, T., Li, M., Mu, G., Hou, T., Zhu, W.G., and Yang, Y. (2019). PKCζ Phosphorylates SIRT6 to Mediate Fatty Acid β-Oxidation in Colon Cancer Cells. Neoplasia *21*, 61–73. https://doi.org/10.1016/j.neo.2018.11.008.
24. Bae, J.S., Park, S.H., Jamiyandorj, U., Kim, K.M., Noh, S.J., Kim, J.R., Park, H.J., Kwon, K.S., Jung, S.H., Park, H.S., et al. (2016). CK2α/CSNK2A1 Phosphorylates SIRT6 and Is Involved in the Progression of Breast Carcinoma and Predicts Shorter Survival of Diagnosed Patients. Am. J. Pathol. *186*, 3297–3315. https://doi.org/10.1016/j.ajpath.2016.08.007.
25. Wan, J., Zhan, J., Li, S., Ma, J., Xu, W., Liu, C., Xue, X., Xie, Y., Fang, W., Chin, Y.E., and Zhang, H. (2015). PCAF-primed EZH2 acetylation regulates its stability and promotes lung adenocarcinoma progression. Nucleic Acids Res. *43*, 3591–3604. https://doi.org/10.1093/nar/gkv238.
26. Chen, Y., Huang, Q., Liu, W., Zhu, Q., Cui, C.P., Xu, L., Guo, X., Wang, P., Liu, J., Dong, G., et al. (2018). Mutually exclusive acetylation and ubiquitylation of the splicing factor SRSF5 control tumor growth. Nat. Commun. *9*, 2464. https://doi.org/10.1038/s41467-018-04815-3.
27. Jin, J., Zhang, L., Li, X., Xu, W., Yang, S., Song, J., Zhang, W., Zhan, J., Luo, J., and Zhang, H. (2022). Oxidative stress-CBP axis modulates MOB1 acetylation and activates the Hippo signaling pathway. Nucleic Acids Res. *50*, 3817–3834. https://doi.org/10.1093/nar/gkac189.
28. Michishita, E., McCord, R.A., Berber, E., Kioi, M., Padilla-Nash, H., Damian, M., Cheung, P., Kusumoto, R., Kawahara, T.L., Barrett, J.C., et al. (2008). SIRT6 is a histone H3 lysine 9 deacetylase that modulates telomeric chromatin. Nature *452*, 492–496. https://doi.org/10.1038/nature06736.
29. Su, J., Wang, F., Cai, Y., and Jin, J. (2016). The Functional Analysis of Histone Acetyltransferase MOF in Tumorigenesis. Int. J. Mol. Sci. *17*. https://doi.org/10.3390/ijms17010099.
30. Chen, Q.Y., Costa, M., and Sun, H. (2015). Structure and function of histone acetyltransferase MOF. AIMS Biophys. *2*, 555–569. https://doi.org/10.3934/biophy.2015.4.555.
31. Song, J., Chun, S., Lee, J., Kim, D., Kim, Y., and Jang, S. (2011). The Histone Acetyltransferase hMOF Is Overexoressed in Non-small Cell Lung Carcinoma.
32. Chen, Z., Ye, X., Tang, N., Shen, S., Li, Z., Niu, X., Lu, S., and Xu, L. (2014). The histone acetylranseferase hMOF acetylates Nrf2 and regulates anti-drug responses in human non-small cell lung cancer. Br. J. Pharmacol. *171*, 3196–3211. https://doi.org/10.1111/bph.12661.
33. Zhao, L., Wang, D.L., Liu, Y., Chen, S., and Sun, F.L. (2013). Histone acetyltransferase hMOF promotes S phase entry and tumorigenesis in lung cancer. Cell. Signal. *25*, 1689–1698. https://doi.org/10.1016/j.cellsig.2013.04.006.
34. Cea, M., Cagnetta, A., Adamia, S., Acharya, C., Tai, Y.T., Fulciniti, M., Ohguchi, H., Munshi, A., Acharya, P., Bhasin, M.K., et al. (2016). Evidence for a role of the histone deacetylase SIRT6 in DNA damage response of multiple myeloma cells. Blood *127*, 1138–1150. https://doi.org/10.1182/blood-2015-06-649970.
35. Cui, J., Pan, G., He, Q., Yin, L., Guo, R., and Bi, H. (2019). MicroRNA-545 targets ZEB2 to inhibit the development of non-small cell lung cancer by inactivating Wnt/β-catenin pathway. Oncol. Lett. *18*, 2931–2938. https://doi.org/10.3892/ol.2019.10619.
36. You, J., Li, Y., Fang, N., Liu, B., Zu, L., Chang, R., Li, X., and Zhou, Q. (2014). MiR-132 suppresses the migration and invasion of lung cancer cells via targeting the EMT regulator ZEB2. PLoS One *9*, e91827. https://doi.org/10.1371/journal.pone.0091827.

37. Shi, Z.M., Wang, L., Shen, H., Jiang, C.F., Ge, X., Li, D.M., Wen, Y.Y., Sun, H.R., Pan, M.H., Li, W., et al. (2017). Downregulation of miR-218 contributes to epithelial-mesenchymal transition and tumor metastasis in lung cancer by targeting Slug/ZEB2 signaling. Oncogene *36*, 2577–2588. https://doi.org/10.1038/onc.2016.414.

38. Lv, H.L., Li, Z.L., and Song, Y.B. (2019). MicroRNA-507 represses the malignant behaviors of non-small cell lung cancer via targeting zinc finger E-box binding homeobox 2. Eur. Rev. Med. Pharmacol. Sci. *23*, 9955–9964. https://doi.org/10.26355/eurrev_201911_19562.

39. Lin, X., Yang, Z., Zhang, P., Liu, Y., and Shao, G. (2021). miR-154 inhibits migration and invasion of human non-small cell lung cancer by targeting ZEB2. Oncol. Lett. *22*, 612. https://doi.org/10.3892/ol.2021.12873.

40. Li, X., Li, C., Bi, H., Bai, S., Zhao, L., Zhang, J., and Qi, C. (2019). Targeting ZEB2 By microRNA-129 In Non-Small Cell Lung Cancer Suppresses Cell Proliferation, Invasion And Migration Via Regulating Wnt/β-Catenin Signaling Pathway And Epithelial-Mesenchymal Transition. Onco Targets Ther. *12*, 9165–9175. https://doi.org/10.2147/ott.S217536.

41. Duan, X., Fu, Z., Gao, L., Zhou, J., Deng, X., Luo, X., Fang, W., and Luo, R. (2016). Direct interaction between miR-203 and ZEB2 suppresses epithelial-mesenchymal transition signaling and reduces lung adenocarcinoma chemoresistance. Acta Biochim. Biophys. Sin. *48*, 1042–1049. https://doi.org/10.1093/abbs/gmw099.

42. Liu, J., Yu, Z., Xiao, Y., Meng, Q., Wang, Y., and Chang, W. (2018). Coordination of FOXA2 and SIRT6 suppresses the hepatocellular carcinoma progression through ZEB2 inhibition. Cancer Manag. Res. *10*, 391–402. https://doi.org/10.2147/cmar.S150552.

43. Sundaresan, N.R., Vasudevan, P., Zhong, L., Kim, G., Samant, S., Parekh, V., Pillai, V.B., Ravindra, P.V., Gupta, M., Jeevanandam, V., et al. (2012). The sirtuin SIRT6 blocks IGF-Akt signaling and development of cardiac hypertrophy by targeting c-Jun. Nat. Med. *18*, 1643–1650. https://doi.org/10.1038/nm.2961.

44. Zhu, B., Yan, Y., Shao, B., Tian, L., and Zhou, W. (2018). Downregulation of SIRT6 is associated with poor prognosis in patients with non-small cell lung cancer. J. Int. Med. Res. *46*, 1517–1527. https://doi.org/10.1177/0300060517750298.

45. Azuma, Y., Yokobori, T., Mogi, A., Altan, B., Yajima, T., Kosaka, T., Onozato, R., Yamaki, E., Asao, T., Nishiyama, M., and Kuwano, H. (2015). SIRT6 expression is associated with poor prognosis and chemosensitivity in patients with non-small cell lung cancer. J. Surg. Oncol. *112*, 231–237. https://doi.org/10.1002/jso.23975.

46. Bai, L., Lin, G., Sun, L., Liu, Y., Huang, X., Cao, C., Guo, Y., and Xie, C. (2016). Upregulation of SIRT6 predicts poor prognosis and promotes metastasis of non-small cell lung cancer via the ERK1/2/MMP9 pathway. Oncotarget *7*, 40377–40386. https://doi.org/10.18632/oncotarget.9750.

47. Hung, J.Y., Horn, D., Woodruff, K., Prihoda, T., LeSaux, C., Peters, J., Tio, F., and Abboud-Werner, S.L. (2014). Colony-stimulating factor 1 potentiates lung cancer bone metastasis. Lab. Invest. *94*, 371–381. https://doi.org/10.1038/labinvest.2014.1.

48. Wang, D., Kon, N., Lasso, G., Jiang, L., Leng, W., Zhu, W.G., Qin, J., Honig, B., and Gu, W. (2016). Acetylation-regulated interaction between p53 and SET reveals a widespread regulatory mode. Nature *538*, 118–122. https://doi.org/10.1038/nature19759.

49. Friedman, J.R., and Kaestner, K.H. (2006). The Foxa family of transcription factors in development and metabolism. Cell. Mol. Life Sci. *63*, 2317–2328. https://doi.org/10.1007/s00018-006-6095-6.

50. Tang, Y., Shu, G., Yuan, X., Jing, N., and Song, J. (2011). FOXA2 functions as a suppressor of tumor metastasis by inhibition of epithelial-to-mesenchymal transition in human lung cancers. Cell Res. *21*, 316–326. https://doi.org/10.1038/cr.2010.126.

51. North, B.J., Marshall, B.L., Borra, M.T., Denu, J.M., and Verdin, E. (2003). The human Sir2 ortholog, SIRT2, is an NAD+-dependent tubulin deacetylase. Molecular cell *11*, 437–444. https://doi.org/10.1016/s1097-2765(03)00038-8.

52. Campeau, E., Ruhl, V.E., Rodier, F., Smith, C.L., Rahmberg, B.L., Fuss, J.O., Campisi, J., Yaswen, P., Cooper, P.K., and Kaufman, P.D. (2009). A versatile viral system for expression and depletion of proteins in mammalian cells. PLoS One *4*, e6529. https://doi.org/10.1371/journal.pone.0006529.

53. Ran, F.A., Hsu, P.D., Wright, J., Agarwala, V., Scott, D.A., and Zhang, F. (2013). Genome engineering using the CRISPR-Cas9 system. Nat. Protoc. *8*, 2281–2308. https://doi.org/10.1038/nprot.2013.143.

54. Stewart, S.A., Dykxhoorn, D.M., Palliser, D., Mizuno, H., Yu, E.Y., An, D.S., Sabatini, D.M., Chen, I.S., Hahn, W.C., Sharp, P.A., et al. (2003). Lentivirus-delivered stable gene silencing by RNAi in primary cells. RNA *9*, 493–501. https://doi.org/10.1261/rna.2192803.

55. Martin, M. (2011). Cutadapt Removes Adapter Sequences from High-Throughput Sequencing Reads, *17*, p. 3. https://doi.org/10.14806/ej.17.1.200.

56. Dobin, A., Davis, C.A., Schlesinger, F., Drenkow, J., Zaleski, C., Jha, S., Batut, P., Chaisson, M., and Gingeras, T.R. (2013). STAR: ultrafast universal RNA-seq aligner. Bioinformatics *29*, 15–21. https://doi.org/10.1093/bioinformatics/bts635.

57. Liao, Y., Smyth, G.K., and Shi, W. (2014). featureCounts: an efficient general purpose program for assigning sequence reads to genomic features. Bioinformatics *30*, 923–930. https://doi.org/10.1093/bioinformatics/btt656.

58. Love, M.I., Huber, W., and Anders, S. (2014). Moderated estimation of fold change and dispersion for RNA-seq data with DESeq2. Genome Biol. *15*, 550. https://doi.org/10.1186/s13059-014-0550-8.

STAR★METHODS

KEY RESOURCES TABLE

REAGENT or RESOURCE	SOURCE	IDENTIFIER
Antibodies		
Anti-SIRT6	Cell Signaling Technology	Cat#2590; RRID:AB_2188926
Anti-FLAG-tag	Sigma-Aldrich	Cat#F7425; RRID:AB_439687
Anti-Myc-tag	Cell Signaling Technology	Cat#2278; RRID:AB_490778
Anti-acetyl-lysine	Millipore	Cat#AB3879; RRID:AB_570574
Anti-MOF	Abcam	Cat#ab200660; RRID:AB_2891127
Anti-β-actin	Sigma-Aldrich	Cat#A5316; RRID:AB_476743
Anti-GST-tag	Abcam	Cat#ab9085; RRID:AB_306993
Anti-HA-tag	Abcam	Cat#ab9110; RRID:AB_307019
Anti-His-tag	Santa Cruz	Cat#sc-8036; RRID:AB_627727
Anti-HDAC1	Santa Cruz	Cat#sc-8410; RRID:AB_627703
Anti-Histone H3	Cell Signaling Technology	Cat#3638; RRID:AB_1642229
Anti-H3K9ac	Cell Signaling Technology	Cat#07-352; RRID:AB_310544
Anti-H3K56ac	Abcam	Cat#ab71956; RRID:AB_10861799
Anti-H3K56ac	Cell Signaling Technology	Cat#07-677; RRID:AB_390167
Anti-ZEB2	Proteintech	Cat#14026-1-AP; RRID:AB_2878001
Anti-FOXA2	Abcam	Cat#ab108422; RRID:AB_11157157
Anti-GAPDH	Proteintech	Cat#60004-1; RRID:AB_2107436
Goat Anti-Mouse IgG (H+L)	Thermo	Cat#31430; RRID:AB_228307
Rabbit Anti-Goat IgG (H+L)	Thermo	Cat#31402; RRID:AB_228395
Donkey Anti-Mouse IgG (H+L) Alexa Fluor 488	Invitrogen	Cat#A21202; RRID:AB_141607
Bacterial and virus strains		
Rosetta (DE3) Competent Cells	Sigma-Aldrich	Cat#70954
Biological samples		
NSCLC patient tissues	Guangdong Provincial People's Hospital	N/A
Chemicals, peptides, and recombinant proteins		
Geneticin Selective Antibiotic (G418 Sulfate)	Thermo Fisher	Cat#10-131-027
Zeocin™ Selection Reagent	Gibco	Cat#R250-01
Opti-MEM® Medium	Gibco	Cat#31985070
polyethyleneimine (PEI)	Polysciences	Cat#23966-1
Lipofectamine® 2000 Reagent	Invitrogen	Cat#11668-019
phosphatase inhibitor cocktail	Roche	Cat#04906837
Protease inhibitor cocktail	Roche	Cat#04693132001
Anti-FLAG® M2 Magnetic Beads	Sigma-Aldrich	Cat#M8823
Recombinant Protein G Agarose Beads	Invitrogen	Cat#15920-010
FLAG peptide	GL Biochem	Cat#180688
4x Laemmli Sample Buffer	Bio-Rad	Cat#1610747
NP-40	Calbiochem	Cat#492015
Triton-X 100	Sigma-Aldrich	Cat#T8787
Nicotinamide	Sigma-Aldrich	Cat#72340
Sodium butyrate	Sigma-Aldrich	Cat#B5887
NAD^+ solution	Sigma-Aldrich	Cat#N1663
Cycloheximide	Sigma-Aldrich	Cat#01810
Tween 20	Sigma-Aldrich	Cat#P1379

(*Continued on next page*)

Continued

REAGENT or RESOURCE	SOURCE	IDENTIFIER
SuperSignal West Pico PLUS ECL Substrate	Thermo Fisher	Cat#34580
RNAiso Plus	Takara	Cat#9109
TB Green Premix Ex Taq	Takara	Cat#RR420A
Lenti-X Concentrator	Takara	Cat#631232
Resazurin Sodium Salt Powder	Sigma-Aldrich	Cat#R7017
Fluorescence Mounting Medium	Dako	Cat#S3023
Propidium Iodide Solution	BioLegend	Cat#421301
RNase A	Sigma-Aldrich	Cat#R4875
Critical commercial assays		
High-Capacity cDNA Reverse Transcription Kit	Applied Biosystem	Cat#4374966
QuikChange II XL Site-Directed Mutagenesis Kit	Agilent Technologies	Cat#200522
SimpleChIP® Enzymatic Chromatin IP Kit	Cell Signaling	Cat#91820
Deposited data		
Raw RNA-sequencing data	this study	GEO: GSE212057
Experimental models: Cell lines		
HEK293	ATCC	CRL-1573
A549	ATCC	CCL-185
H1299	ATCC	CRL-5803
Experimental models: Organisms/strains		
Mouse: BALB/C-NUDE	SLAC	Strain# BALB/cASlac-nu
Oligonucleotides		
Human MOF siRNA	Santa Cruz	Cat#SC-37129
Human MOF shRNA: CGAAAT TGATGCCTGGTATTT	This paper	N/A
Human ZEB2 shRNA: CCCAC CATGAATAGTAATTTA	This paper	N/A
Human HDAC1 sgRNA-1: CACCGCGACATGTTATCT GGACGGA	This paper	N/A
qRT-PCR Primer: Human ZEB2 Forward: AACCATGAGTCCTCCCCACA	This paper	N/A
qRT-PCR Primer: Human ZEB2 Reverse: GTCTTCCTTCATTTCTTCTGGACC	This paper	N/A
qRT-PCR Primer: Human Actin Forward: ACAGAGCCTCGCCTTTGC	This paper	N/A
qRT-PCR Primer: Human Actin Reverse: ATCATCCATGGTGAGCTGGC	This paper	N/A
ChIP-qRT-PCR Primer: Human ZEB2 Promoter Region 1 Forward: GAAGGGAGGGAGGTGGAATTT	This paper	N/A
ChIP-qRT-PCR Primer: Human ZEB2 Promoter Region 1 Reverse: CGCCAAGTTTCTCTCTGGGAA	This paper	N/A
ChIP-qRT-PCR Primer: Human ZEB2 Promoter Region 2 Forward: ACTATCTGGATTGAGGACCCG	This paper	N/A
ChIP-qRT-PCR Primer: Human ZEB2 Promoter Region 2 Reverse: TGGCATCATTATCCTCATCACT	This paper	N/A
Recombinant DNA		
FLAG-SIRT6	North et al.[51]	Addgene plasmid # 13817

(*Continued on next page*)

Continued

REAGENT or RESOURCE	SOURCE	IDENTIFIER
FLAG-SIRT6 H133Y	Tennen et al.[9]	N/A
FLAG-SIRT6 domain deletion mutants (ΔC, ΔN, core, CTE, NTE)	Tennen et al.[9]	N/A
FLAG-SIRT6 mutation (K17R, K128R, K160R, K170R, K245R, K267R, K300R, K128/160R, K128/267R, K160/267R, K3R, K3Q)	This paper	N/A
Myc-MOF	This paper	N/A
Myc-MOF K274R	This paper	N/A
FLAG-HATs (MOF, Tip60, GCN5)	This paper	N/A
HA-p300	This paper	N/A
His-HDAC1	This paper	N/A
FLAG-HDACs (HDAC1-5)	This paper	N/A
FLAG-HDAC1 H141A	This paper	N/A
HA-SIRT1	This paper	N/A
HA-SIRT1 H363Y	This paper	N/A
GST-MOF	This paper	N/A
pET–28a (+)	Novagen	Cat#69864
His-SIRT6	This paper	N/A
His-HDAC1	This paper	N/A
His-HDAC2	This paper	N/A
pLenti-CMV-GFP-Neo	Campeau et al.[52]	Addgene plasmid #17447
pLenti-CMV-GFP-Zeo	Campeau et al.[52]	Addgene plasmid #17449
pLenti-CMV-SIRT6-Neo	This paper	N/A
pLenti-CMV-MOF-Zeo	This paper	N/A
pLenti-CMV-ZEB2-Zeo	This paper	N/A
PX459	Ran et al.[53]	Addgene plasmid #62988
PX459-*HDAC1*-KO	This paper	N/A
pLKO.1	Stewart et al.[54]	Addgene plasmid #8453
pLKO.1-shMOF	This paper	N/A
pLKO.1-shZEB2	This paper	N/A
Software and algorithms		
GraphPad Prism	GraphPad	https://www.graphpad.com
Other		
None	None	None

RESOURCE AVAILABILITY

Lead contact

Further information and requests for resources and reagents should be directed to and will be fulfilled by the lead contact, Zhongjun Zhou (zhongjun@hku.hk).

Materials availability

All unique/stable reagents generated in this study are available from the lead contact without restriction.

Data and code availability

- The raw RNA-sequencing data have been deposited at the Gene Expression Omnibus (GEO) and are publicly available with the accession number GSE212057.
- This paper does not report original code.
- Any additional information required to reanalyze the data reported in this paper is available from the lead contact upon request.

EXPERIMENTAL MODEL AND SUBJECT DETAILS

NSCLC patient samples

All NSCLC tissues and paired normal tissues were obtained from Guangdong Provincial People's Hospital & Guangdong Academy of Medical Sciences, Guangzhou, China. All patients are male. Informed written consent was obtained from all patients. Our study was approved by the Ethics Committee of Guangdong Provincial People's Hospital (Guangzhou, China).

Cell lines

HEK293, A549, and H1299 cells were obtained from American Type Culture Collection (ATCC). HEK293 cells were maintained in Dulbecco's modified Eagle medium (Gibco, 12-800-017), A549 and H1299 cells were maintained in RPMI-1640 (Sigma-Aldrich, Cat: #R6504) and. All culture mediums were supplemented with 10% fetal bovine serum (Gibco, Cat: 10270106) and cells were cultured at 37°C with 5% CO_2.

HDAC1 knockout HEK293 cells were generated by transient transfection of PX459-*HDAC1*-KO plasmid followed by selection with puromycin. A549 and H1299 cells stably expressing FLAG-SIRT6 WT, FLAG-SIRT6 K3R, FLAG-SIRT6 K3Q, Myc-MOF or ZEB2 were generated by infecting with lentivirus followed by selection with geneticin or zeocin.

METHOD DETAILS

Plasmid constructs and siRNA

pcDNA3.1-SIRT6-FLAG (#13817) was purchased from Addgene. FLAG-tagged SIRT6 catalytically inactive mutant and domain deletion mutant constructs of SIRT6 were kindly provided by Dr. Katrin Chua (Stanford School of Medicine, USA). Myc-MOF was made by cloning the human MOF coding sequence into the pcDNA3.1-Myc-His vector. FLAG-MOF, FLAG-GCN5, and FLAG-Tip60 were made by cloning indicated coding sequence into pcDNA3-FLAG vector. HA-p300 was a gift from Dr. Zhenkun Lou (Mayo Clinic College of Medicine, USA). FLAG-SIRT6, Myc-MOF, and FLAG-HDAC1 mutants were constructed by site-specific mutagenesis using QuikChange II XL Site-Directed Mutagenesis Kit (Agilent Technologies, #200522) according to the manufacturer's instructions. HA-tagged wild-type and catalytically inactive SIRT1 were made by cloning human SIRT1 coding sequence into pcDNA3.1-HA vector. FLAG-HDAC1-5 were made by cloning human HDAC1-5 coding sequence into pcDNA3-FLAG vector. GST-MOF was made by cloning the corresponding MOF DNA fragments into the pGEX-6p-1 vector. His-SIRT6, His-HDAC1 and His-HDAC2 were made by cloning the corresponding DNA fragments into the pET–28a (+) vector. pLenti-CMV-GFP-Neo (#17447), pLenti-CMV-GFP-Zeo (#17449) were obtained from Addgene. FLAG-SIRT6, Myc-MOF, and ZEB2 plasmids for lentivirus production were made by cloning the corresponding DNA fragments into pLenti-CMV-GFP-Neo or pLenti-CMV-GFP-Zeo vector by replacing the coding sequence of GFP. PX459-*HDAC1*-KO plasmid was made by cloning the target DNA sequence of human HDAC1 into a PX459 vector. All the generated vectors were verified by Sanger sequencing. Small interfering RNA (siRNA) directed against MOF was obtained from Santa Cruz (sc-37129). All shRNA sequences were retrieved from the GPP Web portal (Broad Institute), annealed and cloned into the pLKO.1 vector.

Co-immunoprecipitation and Western bolt

To analyze the interaction between SIRT6 and MOF, FLAG epitope-tagged SIRT6 or MOF was transfected into HEK293 cells using polyethyleneimine (PEI, Polysciences). Cells were harvested and lysed 48 h after transfection with pre-chilled lysis buffer (50 mM Tris pH 7.5, 1 mM EDTA, 350 mM NaCl and 1% NP40) supplemented with phosphatase inhibitor and protease inhibitor cocktail (Roche, Cat: 04693132001). The cell lysates were then transferred to a 1.5 mL Eppendorf tube and briefly sonicated at 25% amplitude for 20 s followed by centrifugation at 15,000 rpm for 15 min at 4°C. After centrifugation, the supernatants were transferred to a new 1.5 mL Eppendorf tube and 10% of the total lysates were saved as input control. The remaining supernatants were supplemented with 40 μL of anti-FLAG M2 beads (Sigma-Aldrich, Cat: #M8823) and rotated overnight at 4°C. Beads were then collected and washed thrice with lysis buffer. Immunoprecipitated proteins were eluted with lysis buffer containing 2 mg/mL FLAG peptide (GL Biochem Cat: 180688). The supernatant containing the immunoprecipitated proteins were then collected and protein samples subjected to western blotting analysis were obtained by adding 4× Laemmli sample buffer (BioRad) into the supernatant and boiled for 10 min. For the analysis of the endogenous interaction between SIRT6 and MOF, 2 μg of corresponding antibodies were added to the supernatant and collected after sonication. The remaining steps followed the same procedures as described above.

For western blotting, cells were washed twice with PBS to remove residual culture medium. Cells were then lysed by directly adding 2× Laemmli sample buffer (BioRad) containing protease inhibitor cocktail (Roche, Cat: 04693132001) into the culture dish and then lysed for 10 min on a rotator at 4°C. The cell lysates were then transferred to a 1.5 mL Eppendorf tube and boiled at 100°C for 15 min followed by centrifugation at 13,000 rpm for 1 min. A desired amount of cell lysates was resolved by SDS-PAGE, whereafter the resolved proteins were then transferred onto PVDF membranes (Millipore, Cat: IPVH00010). After overnight incubation, membranes were washed three times with PBST and then incubated with secondary antibody at room temperature for one hour. Membranes were then washed three times with PBST and target proteins were visualized on X-ray films using SuperSignal West Pico PLUS Chemiluminescent Substrate (Thermo Fisher Scientific, Cat: #34580).

In vitro binding assay

To examine the direct interaction between SIRT6 and MOF, 20 μL of Glutathione Sepharose beads (GE Healthcare) were first incubated with approximately 2 μg of recombinant GST proteins or GST-fused human MOF proteins in binding buffer (50 mM Tris-HCl, pH 8.0, 150 mM NaCl) at 4°C for 1 h. The beads were then washed thrice with binding buffer and approximately 2 μg of recombinant His-SIRT6 proteins were added into both tubes. The tubes were then placed on a rotator at 4°C to allow binding overnight. Beads were washed three times with binding buffer and boiled for 10 min to allow the elution of the proteins in 100 μL of Laemmli Loading Buffer (Bio-Rad). The proteins recovered from the beads were then resolved by SDS-PAGE and analyzed by western blotting.

Mass spectrometry-based identification of SIRT6 acetylation sites by MOF

To identify the MOF target acetylation sites on SIRT6, HEK293 cells cultured in 15 cm-dish were co-transfected with Myc-MOF and FLAG-SIRT6 for 48 h. Cells were then lysed with lysis buffer (50 mM Tris pH 7.5, 1 mM EDTA, 500 mM NaCl, and 1% NP40) supplemented with protease inhibitor cocktail, followed by a brief sonication to release all the nuclear proteins. After centrifugation at 12,000 rpm for 15 min at 4°C, the supernatants containing the whole cell lysates were incubated with anti-FLAG beads (Sigma-Aldrich, Cat: #M8823) overnight at 4°C. The beads were then washed with lysis buffer five times. The enriched FLAG-SIRT6 proteins were eluted from the beads with lysis buffer containing 2 mg/mL FLAG peptide. The immuno-purified FLAG-SIRT6 were then resolved in 10% SDS-PAGE gel and stained with Coomassie blue solution. The bands corresponding to SIRT6 were cut down and subjected to LC–MS/MS for analysis.

Protein purification

For histone purification from cells, cells were lysed in histone extraction buffer (50 mM Tris-HCl, pH 8.0, 150 mM NaCl, 0.5% Triton X-100) supplemented with protease inhibitor cocktail for 10 min at a 4°C on a rotator. Cell lysates were centrifuged at 2, 000 rpm for 10 min at 4°C and the supernatant was aspirated. The pellets were washed once with pre-chilled histone extraction buffer and re-suspended in 200 μL of 0.2 N HCl to extract histone overnight. The samples were then centrifuged at 2, 000 rpm for 10 min at 4°C and the supernatant containing the extracted histone was collected and stored at −80°C.

The construction of plasmids used for protein purification was as described above. The plasmids were transformed into *Escherichia coli* strain Rosetta DE3 (Novagen) and the expression of recombinant proteins was induced by 0.3 mM IPTG at 16°C overnight. The bacteria were collected by centrifugation at 4, 000 rpm for 30 min and re-suspended in Buffer A (20 mM Tris, 150 mM NaCl, pH 7.4). After brief sonication (in the presence of lysozyme and PMSF), the supernatant containing the recombinant proteins was collected by centrifugation at 18, 000 rpm for 40 min at 4°C. Purification of recombinant proteins was achieved by incubating the supernatant with glutathione agarose beads (Thermo Scientific, #16101) or Ni-NTA Agarose (Thermo Scientific, R90115) at 4°C for 1 hour. The beads were then washed thrice and the recombinant proteins were eluted in Buffer B (20 mM Tris, 150 mM NaCl, 50 mM glutathione or 250 mM imidazole, pH 7.4) at 4°C for 30 min. The eluted protein was concentrated with Amicon Ultra-4 filter (Millipore, UFC801024) and a final concentration of 25% glycerol was added for storage at −80°C.

In vitro deacetylation assay

For histone deacetylation assay, approximately 5 μg of eluted wild-type or mutated FLAG-SIRT6 was incubated with 2 μg of purified histones from HEK293 cells in deacetylation assay buffer (50 mM Tris-HCl, pH 8.0, 150 mM NaCl, 4 mM $MgCl_2$, 2 mM NAD^+ and 1 mM DTT) to make the final volume 50 μL for 4 hours at 30°C. After incubation, 4× Laemmli sample buffer (BioRad) was added to the sample. The samples were then boiled for 15 min and directly subjected to western blotting analysis. The eluted SIRT6 was obtained by overexpressing FLAG-tagged wild-type or mutated SIRT6 in HEK293 cells followed by a FLAG pull-down using anti-FLAG beads (Sigma-Aldrich, Cat: #M8823). The FLAG-tagged SIRT6 proteins were then eluted with 2 mg/mL FLAG peptide (GL Biochem Cat: 180688).

For the SIRT6 deacetylation assay, FLAG-SIRT6 was co-expressed with Myc-MOF in HEK293 cells followed by elution with FLAG peptide and used as the substrate for the assay. Eluted FLAG-SIRT6 was incubated with about 2 μg of purified His-HDAC1 or His-HDAC1 in the deacetylation assay buffer (10 mM Tris–HCl pH 8.0, 10 mM NaCl) at 30°C for 4 hours. The reaction mixtures were then resolved by SDS-PAGE and analyzed by western blotting.

Establishment of stable knockout cells using the CRISPR/Cas9 system

Single guide RNA (sgRNA) target sequences of *HDAC1* were cloned into the PX459 vector system after annealing. HEK293 cells were transiently transfected with PX459-*HDAC1*-KO plasmid and treated with puromycin 24 hours post-transfection to allow the selection of successfully transfected cells for 48 hours. Cells were then seeded in a very low density to allow single colony formation. Single colonies were then picked and cell lysates were collected subject to western blotting to check the HDAC1 protein level.

RNA-sequencing

Total RNA was prepared using RNAiso Plus (Cat: #9109) following the manufacturer's instructions. After library construction, the library were sequenced using illumina HiSeq X Ten platform and 150 bp paired-end reads were generated. The library construction and the RNA-sequencing were conducted by NOVOGENE (HK) COMPANY LIMITED.

Bioinformatics pipeline

Raw reads were first checked for quality with FastQC (Babraham Bioinformatics) followed by trimming of the adapters (12 bp) with Cutadapt.[55] Thereafter, alignment to the Human Genome Reference Consortium Human Build 38 (GRCh38) was carried out with STAR.[56] Then, transcript abundance was summarized at the gene level with featureCounts[57] to generate an expression matrix. Only genes with a total of at least three reads across all the samples were considered for differential expression analysis with DESeq2.[58] Genes with an adjusted *p-value* <0.05 and $|\log2(\text{fold change})| > \log_2(1.5) = 0.58$ were considered as differentially expressed. The top five DEGs were ranked by the adjusted *p-value*.

Quantitative PCR

The total RNA from cells was prepared using RNAiso Plus (Cat: #9109) following the manufacturer's instructions. For reverse transcription, 1 μg of total isolated RNA was used to generate cDNA using High-Capacity cDNA Reverse Transcription Kit (Applied Biosystems Cat: #4374966). quantitative-PCR (qPCR) reactions were performed with the StepOnePlus Real-Time PCR System in a 96-well format. The reaction mixture was made with TAKARA TB Green Premix Ex Taq (Cat: #RR420A). For each sample, triplicate reactions were performed and the expression level of interested markers was normalized to actin levels.

Immunofluorescence staining

For immunofluorescence staining, cells were plated on glass coverslips and cultured in 24-well plates. After aspirating the culture medium, cells were fixed with 4% paraformaldehyde in PBS at room temperature for 15 min. Cells were washed twice with PBS and permeabilized with 0.1% Triton X-100 in PBS at room temperature for 10 min. Cells were then blocked in 5% bovine serum albumin (BSA) in PBS for 1 hour at room temperature. The immuno-staining was achieved by incubating the cells with anti-FLAG antibody diluted in 5% BSA in PBS overnight at 4°C. After washing three times with PBS, cells were incubated with the secondary antibody coupled to AlexaFluor 488 at room temperature for 1 hour. Cells were then washed three times with PBS followed by adding Hoechst 33342 for 1 min at room temperature to observe the nuclei. Cells were then washed three times with PBS followed by mounting with Dako Fluorescence Mounting Medium (Cat: #S3023). The coverslips were then transferred to glass slides and sealed with nail polish. The slides were kept in the dark prior to confocal imaging by Carl Zeiss LSM 780 Confocal Microscope.

Chromatin immunoprecipitation (ChIP) assay

Chromatin Immunoprecipitation (ChIP) assay was performed using SimpleChIP Enzymatic Chromatin IP Kit from Cell Signaling (#91820) (hereinafter referred to as the "Kit") with some modifications. For one ChIP reaction, half of the 15 cm dish of cells were used. Briefly, cells were crosslinked by incubating in 1% formaldehyde at room temperature for 10 min and quenched in 0.125 M glycine for 5 min. After washing twice with ice-cold PBS, the crosslinked cells were scratched out from the culture plate, re-suspended and lysed in ChIP lysis buffer (20 mM Tris-HCl pH 7.5, 85 mM KCl, 1% NP40). Chromatin were digested by directly adding the appropriate amount of micrococcal nuclease (NEB, #M0247) into the cell lysates and incubated in a 37°C water bath for 30 min. A pre-test experiment was carried out to determine the optimized amount of micrococcal nuclease added for one ChIP reaction. In the current experiment, 0.75 μL of micrococcal nuclease was added to digest chromatin from half 15-cm dish of cells. Digestion was stopped by adding 10 mM final concentration of EDTA on ice. Antibodies (2 μg) directed against H3K9ac or H3K56ac and beads (as provided in the Kit) were then added and the immunoprecipitation was performed overnight at 4°C on a rotator. On the following day, beads were washed twice with ChIP lysis buffer and high salt washing buffer (ChIP lysis buffer with 500 mM NaCl). Protein-bound DNA was eluted by adding 150 μL of Elution Buffer (provided in the Kit) and incubated at 65°C on a tube shaker with vortexing (12, 000 rpm). The supernatant was saved and reverse crosslinking was performed by adding 2 μL of proteinase K (20 mg/mL) and thereafter incubated at 65°C overnight. Finally, DNA was purified using the columns as provided by the Kit and subjected to qPCR analysis.

Resazurin cell viability assay

Briefly, A549 and H1299 cells were seeded in 24-well plates at a density of 1×10^4 cells per well. Resazurin solution (44 μM of working concentration was prepared by diluting stock resazurin solution with culture medium) was added to the well every 24 hours followed by incubation at 37°C for 4 hours. After incubation, the medium containing the resazurin solution was transferred to a 96-well plate and the relative fluorescent units (RFU) were measured by employing a plate reader using default settings. To make the 20× stock resazurin solution, 1 g of resazurin sodium salt powder (Cat: #R7017) was resolved in 50 mL PBS whereby the solution was sterile filtered before use.

In vitro colony formation assay

Briefly, A549 and H1299 cells were plated in 6-well plates at a density of 500 cells per well and cultured for 10–14 days with the culture medium changed every three days. The medium was then aspirated and the colonies were stained with 0.1% crystal violet solution. The total number of colonies in each well was determined with ImageJ and used for further analysis.

Propidium iodide staining and cell cycle analysis

Briefly, cells were harvested and washed twice with ice-cold PBS. Cells were then fixed by adding 1 mL 70% cold ethanol dropwise into the tube while vortexing to ensure a complete fixation of all cells and incubated at 4°C for 1 hour. After fixation, cells were

collected by centrifugation at 850*g* for 2 min followed by washing twice with PBS. Cells were then stained with 500 μL PI staining solution (50 μg/mL PI, 10 μg/mL RNase in PBS) in the dark at room temperature for 30 min. The cell cycle analysis was performed with the BD FACSCantoII Analyzer.

Trans-well migration and invasion assays

For cell migration assay, 1×10^5 A549 cells or 2.5×10^4 H1299 cells were seeded in chambers with 8 μm pore size polycarbonate filters containing 0.5 mL serum-free RPMI1640 medium. The chambers were then placed into each well of a 24-well plate containing 0.75 mL full culture medium. Cells were cultured in a 37°C incubator for 24 hours until cell migration was detectable. Cells were then fixed in 4% paraformaldehyde in PBS and stained with 2% crystal violet for 10 min. Cotton tips were then used to remove the unmigrated cells in the upper layer of the filter. The cell number and density representing cell migration ability were measured and calculated by the image analyzer ImageJ. For cell invasion, 2.5×10^4 A549 or H1299 cells were seeded and the steps in the above-described cell migration assay were similarly carried out with the exception that the culture chambers were coated with 10% Matrigel in serum-free RPMI 1640 medium at 37°C overnight. At least three independent experiments were performed to calculate cell migration and invasion rates.

In vivo xenograft tumorigenic assay

Briefly, H1299 cells (5×10^6) were suspended in sterile PBS, mixed with Matrigel (2:1) and then subcutaneously injected into the right flank of 6-week-old female nude mice (n = 10 per group). Tumor sizes were measured every three days using vernier caliper and the tumor volumes were calculated using the formula: volume = (wide^2 × length)/2. Mice were sacrificed 40 days upon injection and the final tumor weight and volume were measured. The protocols in this project were approved by the Committee on the Use of Live Animals in Teaching and Research of the University of Hong Kong and all animal experiments were carried out under the Animals (Control of Experiments) Ordinance of Hong Kong.

Patient tumor samples

To analyze the SIRT6 acetylation levels in NSCLC patient tissues, tumor samples were freshly obtained from NSCLC patients that had received surgery at Guangdong Provincial People's Hospital. The adjacent normal lung tissue samples were obtained simultaneously from the same patients. The tissue samples were immediately collected after surgery, lysed in a homogenizer and subjected to immunoprecipitation assay.

QUANTIFICATION AND STATISTICAL ANALYSIS

The experiment results were analyzed with GraphPad Prism 6 software. The data were quantified and presented as mean ± SEM and two-tailed Student's t-test was performed to assess the statistical significance between the two group means. All images or statistical results were based on at least three independent experiments. *P*-values <0.05 were considered as being statistically significant for all experiments. * represents $P< 0.05$, ** represents $P< 0.01$, and *** represents $P< 0.001$.

ADDITIONAL RESOURCES

Figures S1–S7 can be found at the Supplemental information file related to this paper.